AD-A110 295 SRI INTERNATIONAL MENLO PARK CA F/G 4/1
RADAR TRACKING OF BARIUM ION CLOUDS: RESULTS OF THE PLACES EXPE--ETC(U)
AUG 81 V H GONZALEZ DNA001-79-C-0363

UNCLASSIFIED DNA-5851F NL

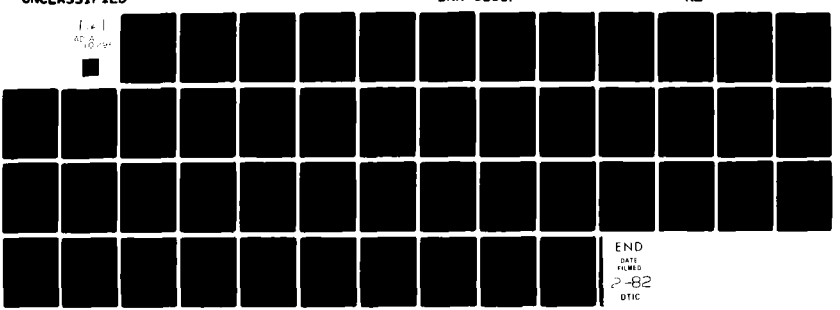

END
DATE FILMED
2-82
DTIC

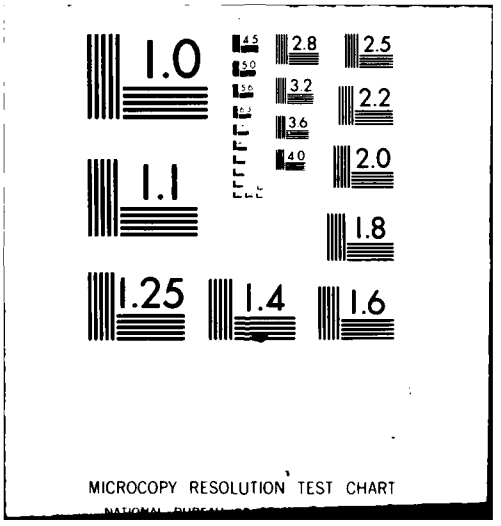
1.0
1.1
1.25
1.4
1.6
1.8
2.0
2.2
2.5
2.8
3.2
3.6
4.0
4.5
5.0
MICROCOPY RESOLUTION TEST CHART

(12) LEVEL

DNA 5851F

RADAR TRACKING OF BARIUM ION CLOUDS: RESULTS OF THE PLACES EXPERIMENT

Victor H. Gonzalez

SRI International
333 Ravenswood Avenue
Menlo Park, California 94025

1 August 1981

Final Report for Period 1 September 1979—1 May 1981

CONTRACT No. DNA 001-79-C-0363

APPROVED FOR PUBLIC RELEASE;
DISTRIBUTION UNLIMITED.

THIS WORK SPONSORED BY THE DEFENSE NUCLEAR AGENCY
UNDER RDT&E RMSS CODE B322079462 I25AAXHX64207 H2590D.

Prepared for
Director
DEFENSE NUCLEAR AGENCY
Washington, D. C. 20305

Destroy this report when it is no longer needed. Do not return to sender.

PLEASE NOTIFY THE DEFENSE NUCLEAR AGENCY, ATTN: STTI, WASHINGTON, D.C. 20305, IF YOUR ADDRESS IS INCORRECT, IF YOU WISH TO BE DELETED FROM THE DISTRIBUTION LIST, OR IF THE ADDRESSEE IS NO LONGER EMPLOYED BY YOUR ORGANIZATION.

UNCLASSIFIED

SECURITY CLASSIFICATION OF THIS PAGE (When Data Entered)

REPORT DOCUMENTATION PAGE		READ INSTRUCTIONS BEFORE COMPLETING FORM
1. REPORT NUMBER DNA 5851F	2. GOVT ACCESSION NO. AD-A110	3. RECIPIENT'S CATALOG NUMBER 295
4. TITLE (and Subtitle) RADAR TRACKING OF BARIUM ION CLOUDS: RESULTS OF THE PLACES EXPERIMENT		5. TYPE OF REPORT & PERIOD COVERED Final Report for Period 1 Sep 79 to 1 May 81
		6. PERFORMING ORG. REPORT NUMBER SRI Project 8780
7. AUTHOR(s) Victor H. Gonzalez		8. CONTRACT OR GRANT NUMBER(s) DNA 001-79-C-0363
9. PERFORMING ORGANIZATION NAME AND ADDRESS SRI International 333 Ravenswood Avenue Menlo Park, California 94025		10. PROGRAM ELEMENT, PROJECT, TASK AREA & WORK UNIT NUMBERS Subtask I25AAXHX642-07
11. CONTROLLING OFFICE NAME AND ADDRESS Director Defense Nuclear Agency Washington, D.C. 20305		12. REPORT DATE 1 August 1981
		13. NUMBER OF PAGES 50
14. MONITORING AGENCY NAME & ADDRESS(if different from Controlling Office)		15. SECURITY CLASS (of this report) UNCLASSIFIED
		15a. DECLASSIFICATION/DOWNGRADING SCHEDULE N/A

16. DISTRIBUTION STATEMENT (of this Report)

Approved for public release; distribution unlimited.

17. DISTRIBUTION STATEMENT (of the abstract entered in Block 20, if different from Report)

18. SUPPLEMENTARY NOTES

This work sponsored by the Defense Nuclear Agency under RDT&E RMSS Code B322079462 I25AAXHX64207 H2590D.

19. KEY WORDS (Continue on reverse side if necessary and identify by block number)

Barium releases	Incoherent scatter
Ion clouds	Striations
Radar tracking	Ionospheric plasmas

20. ABSTRACT (Continue on reverse side if necessary and identify by block number)

This report describes the results of the Radar tracking of the barium ion clouds during the PLACES series of releases. Ion cloud motion, electron density, altitude, and shape are described.

DD FORM 1 JAN 73 1473 EDITION OF 1 NOV 65 IS OBSOLETE

UNCLASSIFIED

SECURITY CLASSIFICATION OF THIS PAGE (When Data Entered)

410241

TABLE OF CONTENTS

LIST OF ILLUSTRATIONS

LIST OF ILLUSTRATIONS (Continued)

BLANK PAGE

I INTRODUCTION

The PLACES communication experiment consisted of a series of high-altitude barium releases that took place at Eglin Air Force Base, Florida. During these experiments, the AN/FPS-85 UHF radar, operating in an incoherent scattering mode, tracked the ionized barium cloud and recorded the measurements that were taken. This mode of measuring electron densities consists of receiving the aggregate reflections from individual electrons that populate the ionized region of interest. The resolution of the radar beam is sufficiently adequate to attain a spatial, as well as temporal description of the ion cloud. This description can be correlated with optical data that were taken during the short optical window. The spatial and temporal description of the ion cloud will assist the interpretation and analysis of data taken in the course of the main experiment, which was the evaluation of communication links during disturbed conditions in the propagating medium.

This report describes the experimental results and a review of the data on a test-by-test basis. The calibration ritual that took place before each experiment will be described in Section II. Sections III, IV, V, and VI will be devoted to the individual tests.

II PRELIMINARY MEASUREMENTS

At the beginning of each test and about 30 min before the launching of the barium payload, a series of measurements designed to calibrate the radar were made. There were two kinds of calibration measurements made: system noise measurements and ionospheric measurements.

Histograms of the system noise and of the system noise plus noise source were made by sampling the ADC output of the radar. Approximately 10^6 samples were obtained for each polarization channel. The ADC output was read directly into the computer through the radar-computer interface (RICE). The numbers obtained from the ADC are those that were translated into electron densities during the cloud tracking exercise.

Figure 1 is an example of the histograms of the system noise and the resulting distribution functions of the horizontal and vertical system noise outputs. These historgrams were repeated for every day of the PLACES series, with the same results indicating good consistency in the performance of the equipment, the horizontal channel histogram agrees very well with the theoretical curve. The theoretical curve results from assuming that the radar front end noise is a Gaussian-distributed amplitude and an ideal logarithmic amplifier, and it is given by the following formula:

$$F(z) = \ell n(10)\ 10^{x}\ e^{-10^{x}}$$

$$x = z - A$$

$$A = \mathrm{Log}(P_o)$$

The vertical channel histogram, on the other hand, shows anomalous spikes at certain equally spaced levels. This is definitely produced by a malfunction in the ADC that persisted throughout the PLACES series. Fortunately, the effect of this malfunction was not very serious and was compensated for by the calibration and the averaging during the tests.

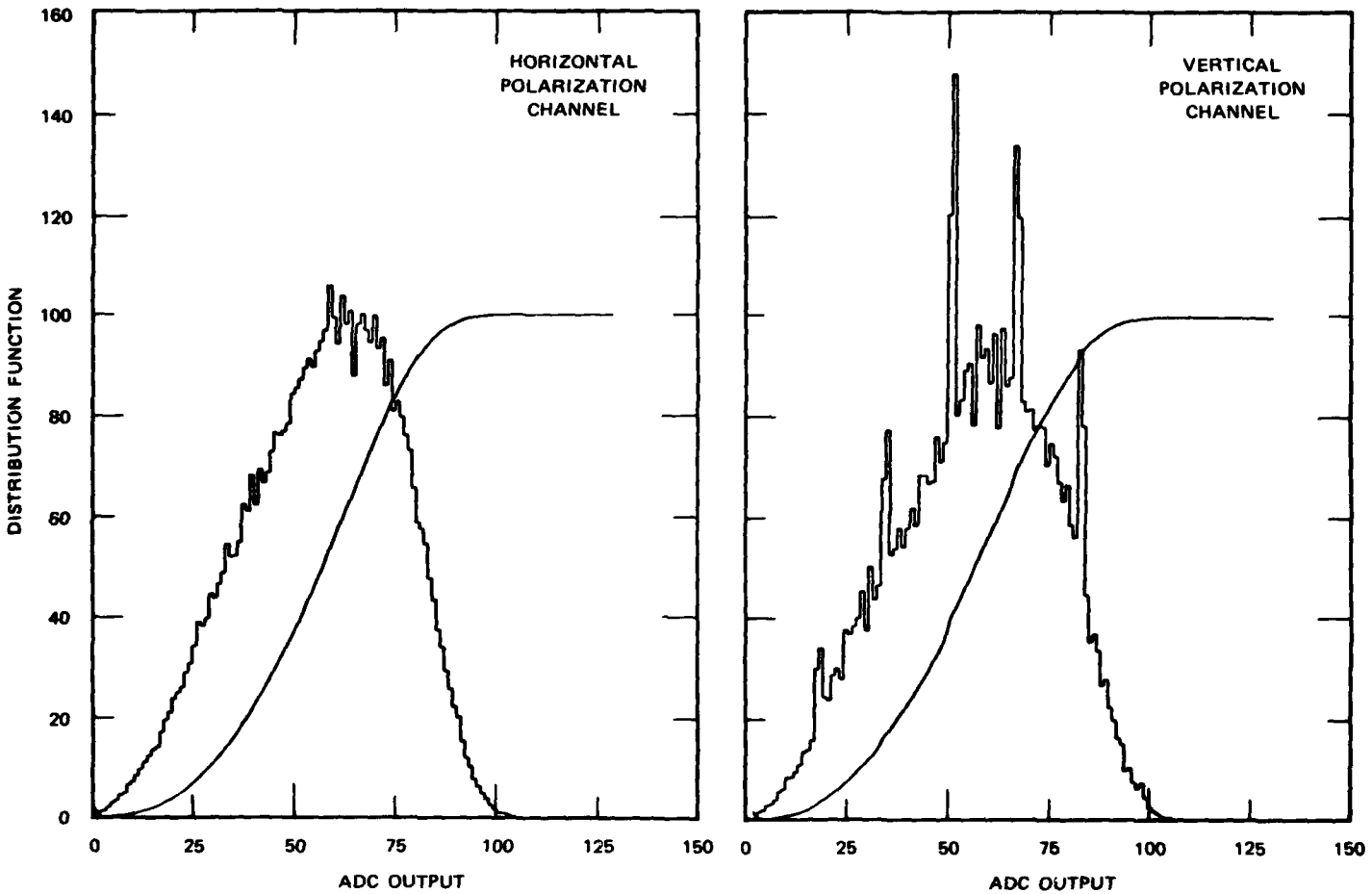

FIGURE 1 SYSTEM NOISE HISTOGRAMS AND DISTRIBUTION FUNCTIONS — EVENT GAIL

The calibration procedure itself is shown in Figure 2. A correspondence is formed between the ADC output numbers and a scale of power normalized to the average front end noise. The basis for the correspondence is equal distribution function values for the measured curved (of Figure 1) and for the theoretical power distribution curve given by:

$$F(p) = 1 - \exp(-p/P_o) \quad .$$

To clarify the procedure, let us assume that N_1 is the ADC number corresponding to a measured distribution function level, F_1. Solving the formula above, we determine the normalized power level p_1/P_o:

$$p_1/P_o = -\mathrm{Ln}(1 - F_1) \quad .$$

In this manner the calibration curve (c) of Figure 2 is formed. Actually, the computer computes and stores the power levels for each ADC level as a look-up calibration table.

This type of calibration is advantageous because it can calibrate output readings below the average noise level. In an incoherent-scatter-type measurement, this calibration is necessary because a large percentage of the samples result in measurements below the average noise power level.

The second type of measurement taken before each test is of the ambient ionosphere. Ionosphere profiles, such as shown in Figure 3, are taken by integration returns from the ionosphere for periods of 2 to 10 min according to the available time. A comparison with the maximum value of f_oF2 values obtained with an ionosonde provides a point of reference in the conversion of normalized power to absolute electron densities. Ionosondes are able to measure the critical frequency of the ionosphere with a high degree of accuracy so that the measured constant relating the returned power to the electron density is very reliable.

Figure 4 summarizes the f_oF2 values measured during the hour preceding each event, and verbally transmitted over the experimenter's network.

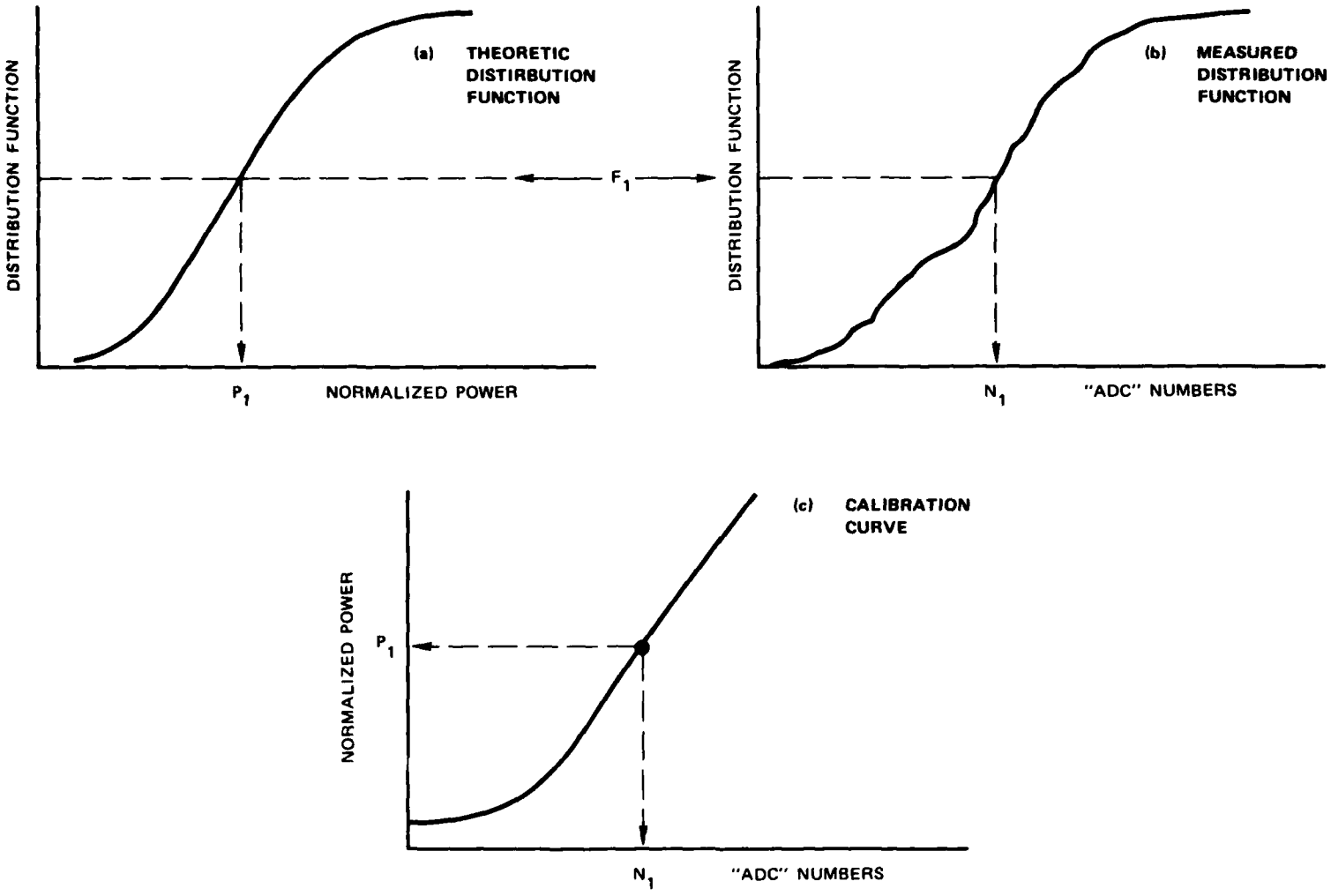

FIGURE 2 USE OF THE NOISE HISTOGRAM TO CALCULATE THE RECEIVER CALIBRATION CURVE

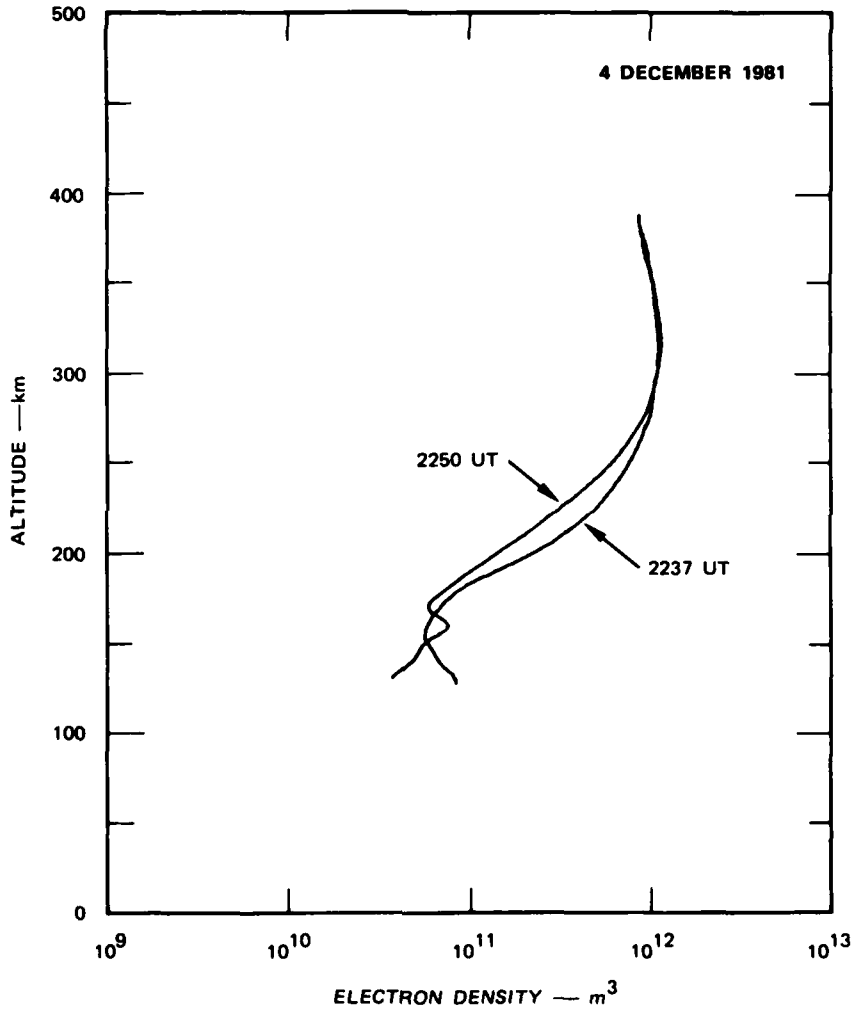

FIGURE 3 IONOSPHERIC PROFILES OBTAINED BEFORE LAUNCHING THE PAYLOAD FOR EVENT GAIL

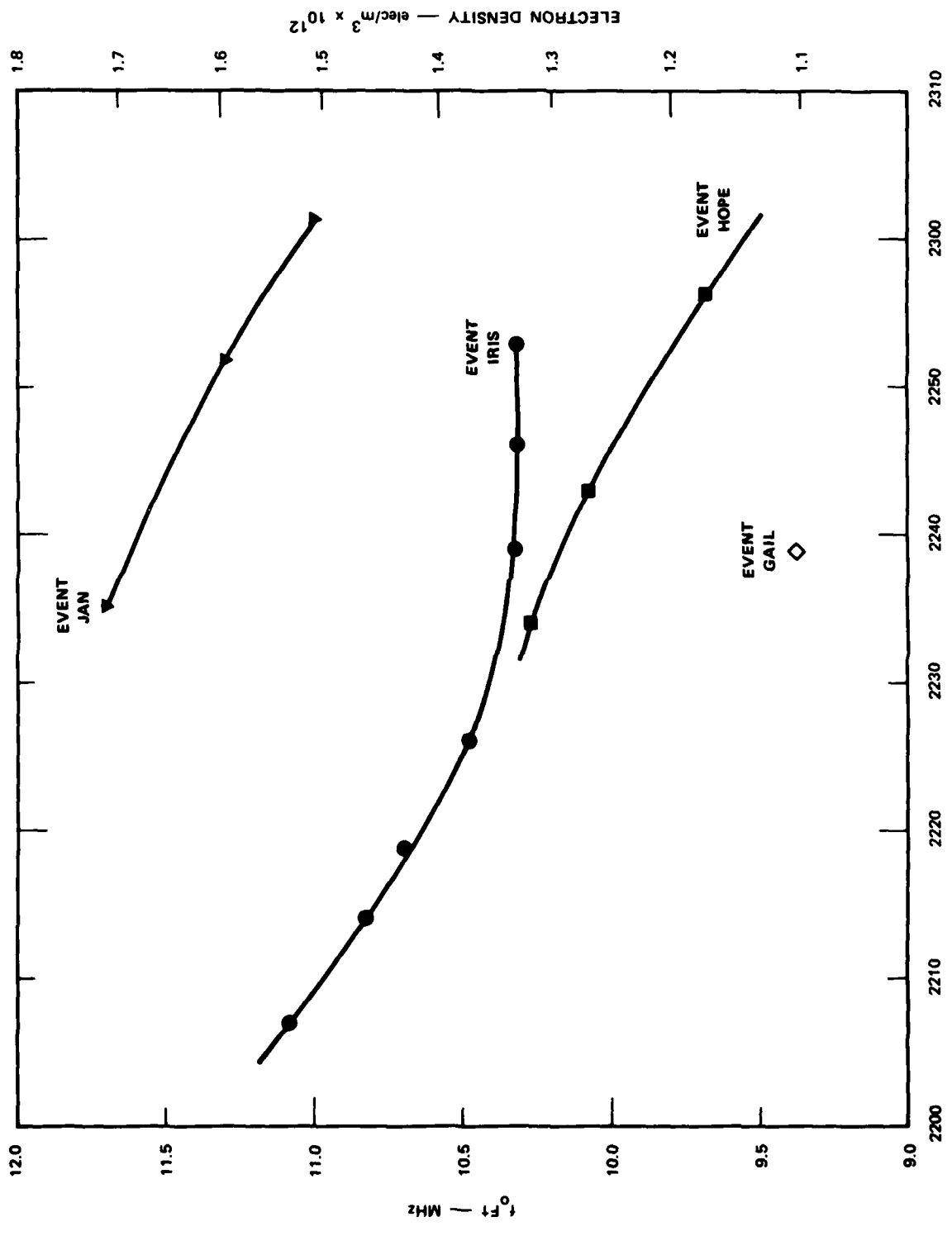

FIGURE 4 f_oF_2 VALUES READ FROM THE IONOSONDE IN REAL TIME

III EVENT GAIL

Event GAIL was tracked for approximately two hours after release. Figure 5 shows the small motion followed by the tracked point of the ion cloud. Except for the first few minutes after release when the track was still not well established. The drift was eastward up to about T + 45 min and westward until the track was interrupted. The northbound motion on the cloud could be caused by a descent of the ion cloud along the magnetic field line or it may be caused by the change of the position of the point with the largest electron density within the cloud itself.

The change of altitude of the ion cloud is shown in Figure 6. The cloud has dropped rapidly, and in two hours descended to an altitude of 125 km. The average vertival rate of descent was 7.8 m/s, and the initial downward velocity was 23 m/s.

Figure 6 also shows, by the spread of the data points in altitude, the times at which the tracking of the ion cloud was good and the times at which it was not. From T + 20 min until T + 130 min, the vertical spread of altitude data was very narrow, indicating that a good track was established during this period. Before the T + 20 min park, a very wide spread in the data points indicates problems in the tracking process. A cable in the radar controlling the sampling of data broke at about the time of release. Data and track were lost during the time necessary to diagnose and solve the problem. When the radar finally began following the proper sequence of measurements to track the cloud, it took some time before zeroing in on the point of greatest electron density.

The time history of the maximum electron density is shown in Figure 7. The small spread of data after T + 20 min is also evident on this graph. The spread in electron density measurements is caused by random errors and by pointing errors. The statistical errors occurred because a limited number of pulses was used for integration at each antenna beam position and these statistical errors were the limit of the accuracy for the

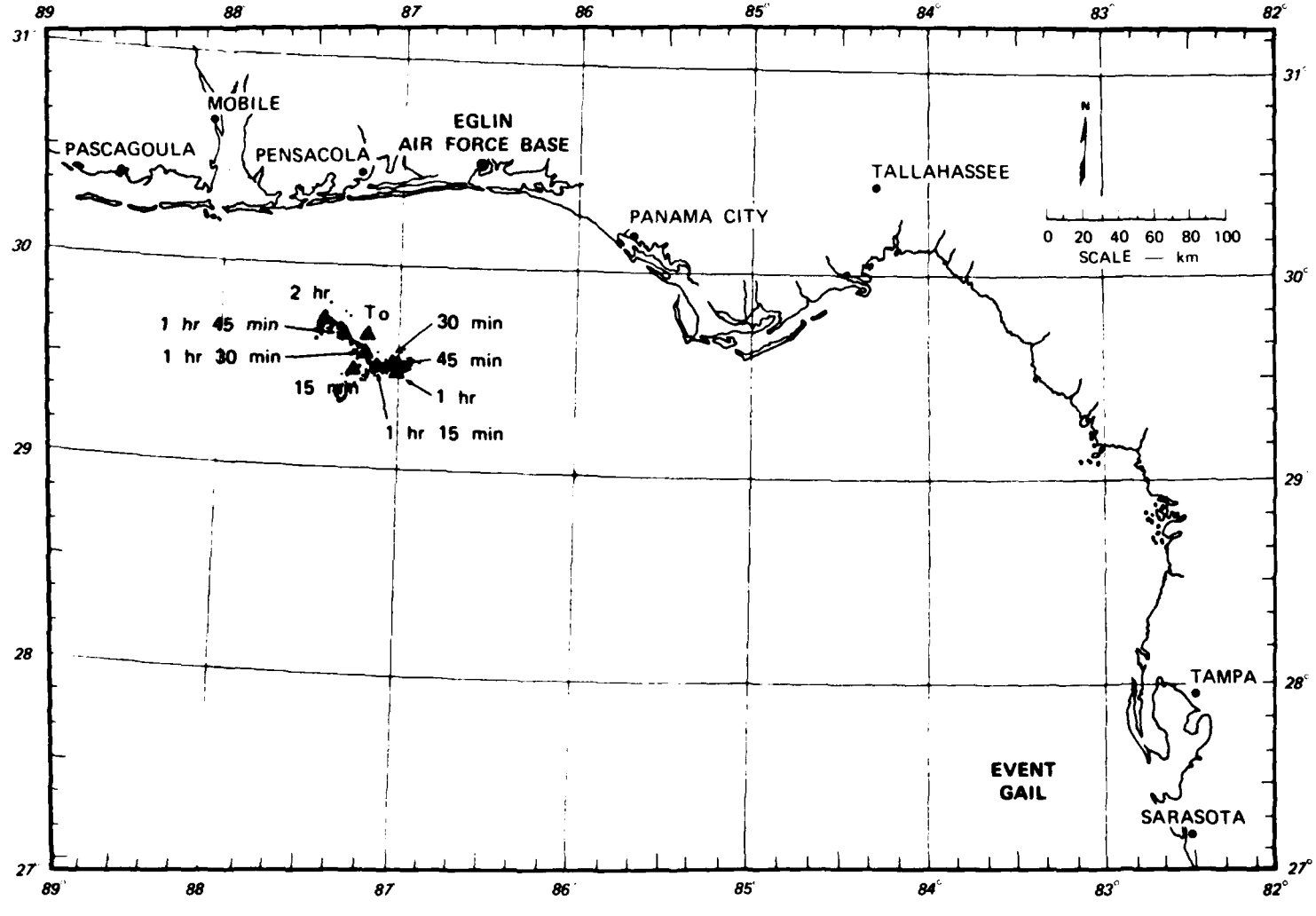

FIGURE 5 HORIZONTAL TRACK OF EVENT GAIL

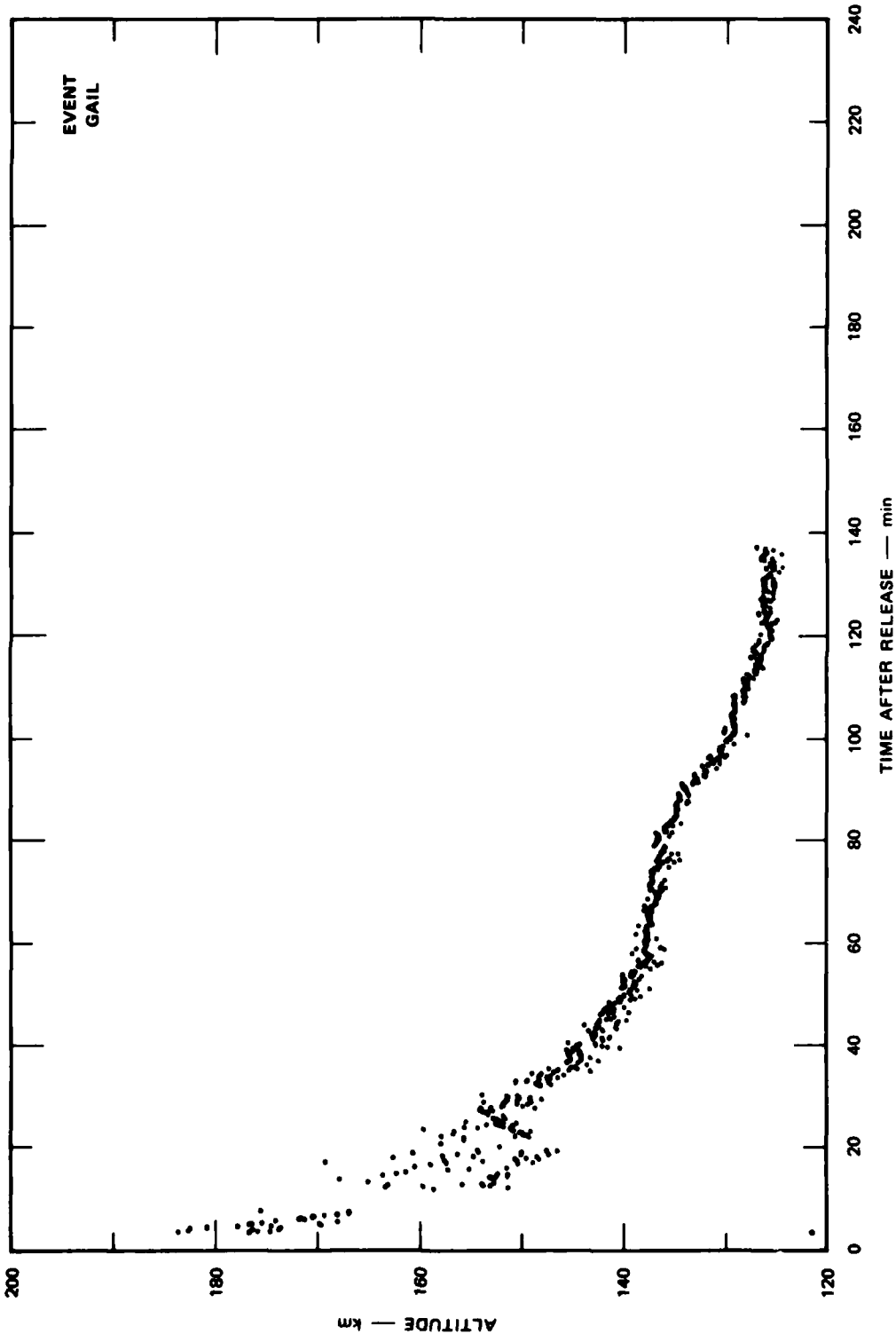

FIGURE 6 ATTITUDE DATA FROM EVENT GAIL

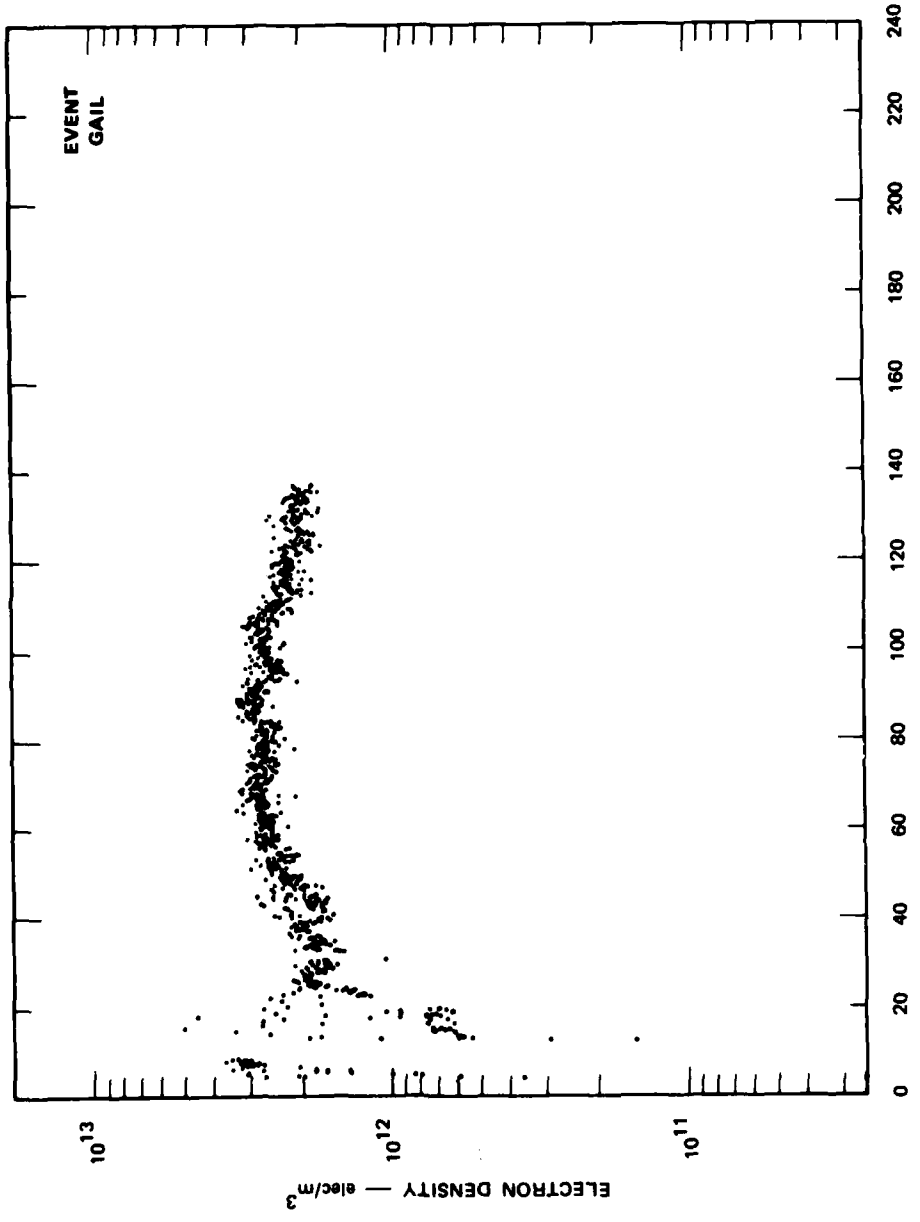

FIGURE 7 MAXIMUM ELECTRON DENSITY AS A FUNCTION OF TIME FOR EVENT GAIL

electron density measurements. The pointing errors on the other hand reflect a limitation in the tracking algorithm which did not always point the antenna beam to the point of maximum electron density. The pointing errors depend on a complicated set of geometric considerations and is difficult to describe; however, they appear to be larger than the random errors in some circumstances. The total spread of points in Figure 7 has a sigma of about 4 to 5%. The main limitation in the electron density measurement is the accuracy of the absolute calibration of the radar.

IV EVENT HOPE

Event HOPE was the smoothest running test from the point of view of radar tracking. The ion cloud was tracked for over 4 hours after release, and good quality data were obtained. The ground track of Event HOPE is shown in Figure 8. There is a monotonic westward motion throughout the life of the ion cloud. There are some reversals of motion in the North-South direction, however, that should be reviewed with care. The southward motion is unquestionably a drift involving ionization that crosses magnetic field lines. The motion to the north may be caused by the vertical fall of the ion cloud with a tendency to slide northward along the magnetic field lines. As has happened in other experiments, the radar sometimes changes the tracked point from one region of the cloud to another, and this tendency could be responsible for the apparent reversal between T + 60 min and T + 75 min.

The vertical descent of the ion cloud shown in Figure 9 indicates a rate of descent of 11 m/s during the first 50 min. The vertical velocity then slowed to only 2.5 m/s and the ion cloud dropped to an altitude of 120 km at four hours after release. Understanding the evolution of an ion cloud and following its changes when it reaches such a low altitude is interesting to researchers on this field.

The maximum electron density shown in Figure 10 shows a remarkably constant value after the first 20 min. This near constant value occurs as the ion cloud changes its altitude by several kilometers. To have confidence in the altitude history of the ion cloud, we have closely examined the quality of the data acquired at times separated by three hours. Figure 11 shows the received power data acquired with 2-s or 80-pulse integration and plotted as a function of altitude. We see that even though the returns from the ion cloud at 227:27 UT are five times smaller than at 2311:51 UT, the returns from the ion cloud are still clearly well defined and definitely above the noise level. Figure 12

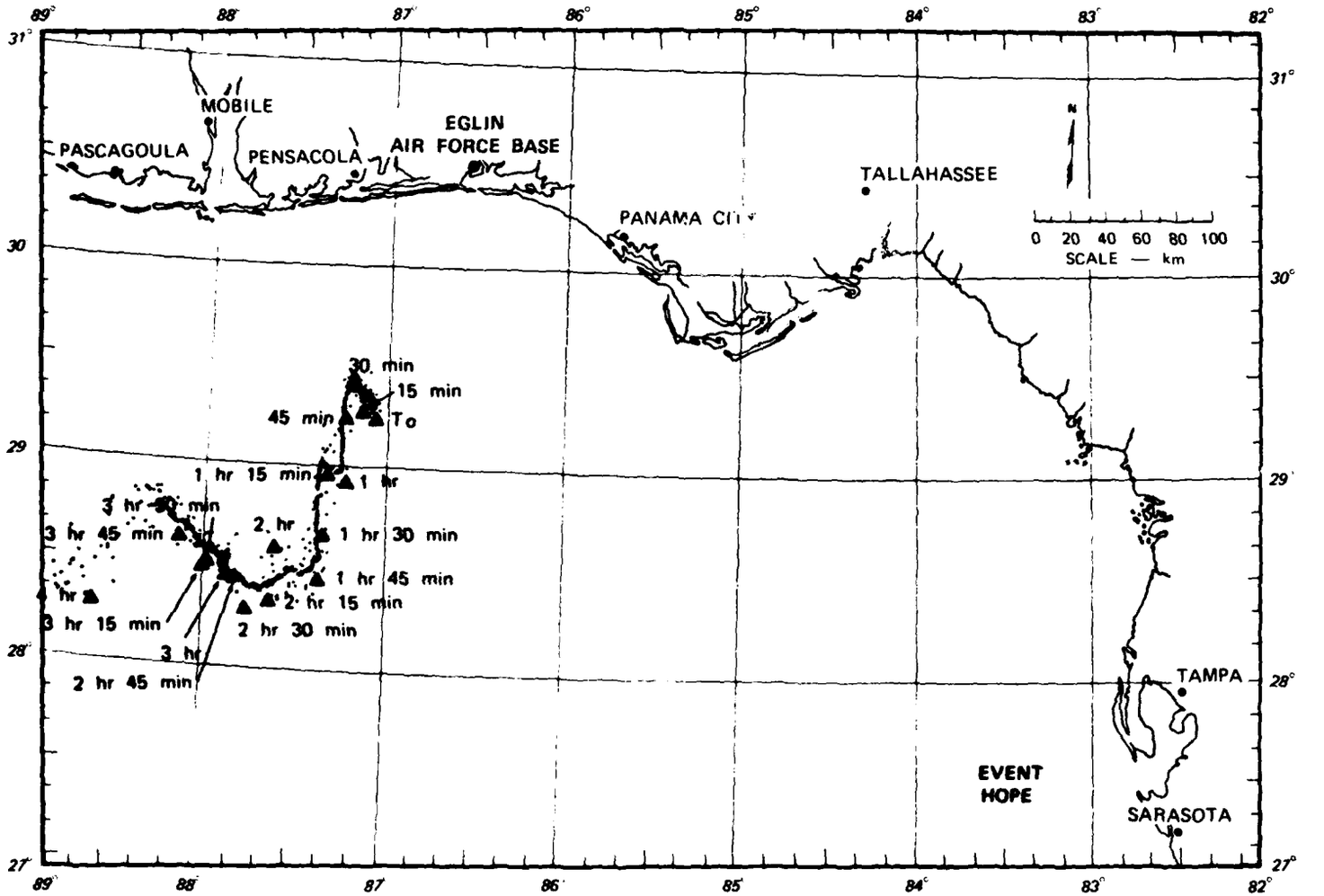

FIGURE 8 HORIZONTAL TRACK OF EVENT HOPE

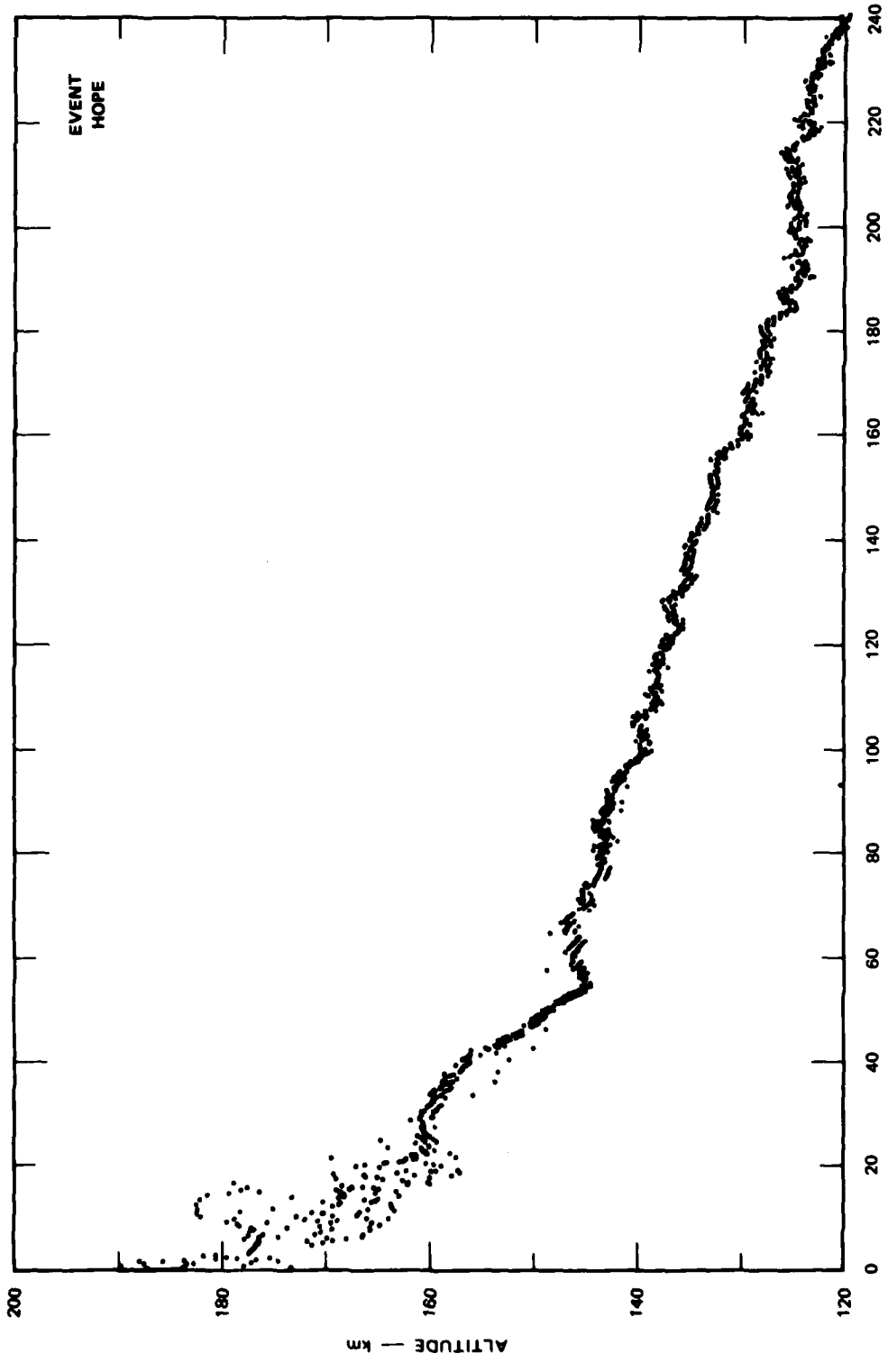

FIGURE 9 ALTITUDE DATA AS A FUNCTION OF TIME OF EVENT HOPE

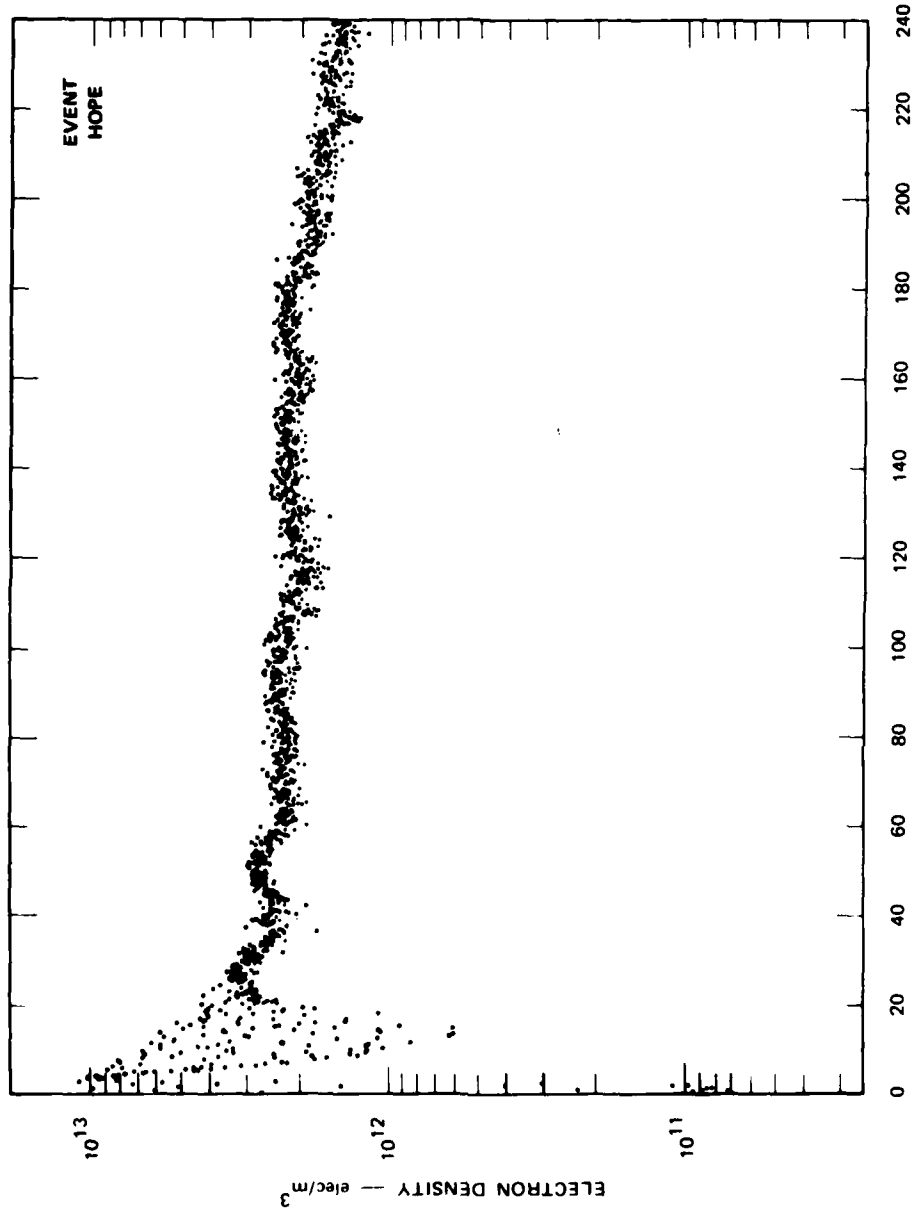

FIGURE 10 MAXIMUM ELECTRON DENSITY AS A FUNCTION OF TIME FOR EVENT HOPE

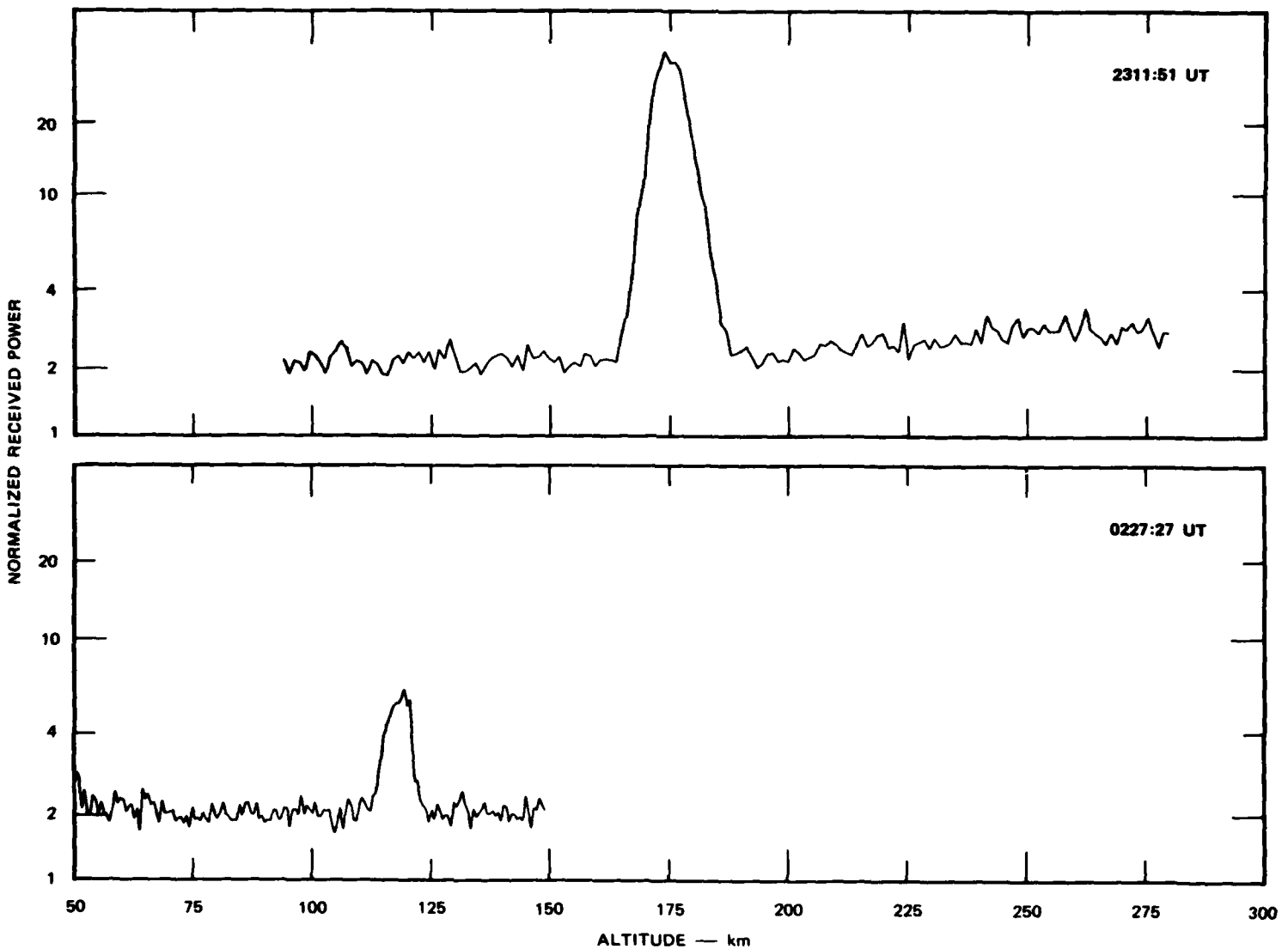

FIGURE 11 ROUGH DATA ACQUIRED FOR TWO ANTENNA-BEAM POSITIONS WITH TWO-SECOND INTEGRATION TIME OF EVENT HOPE

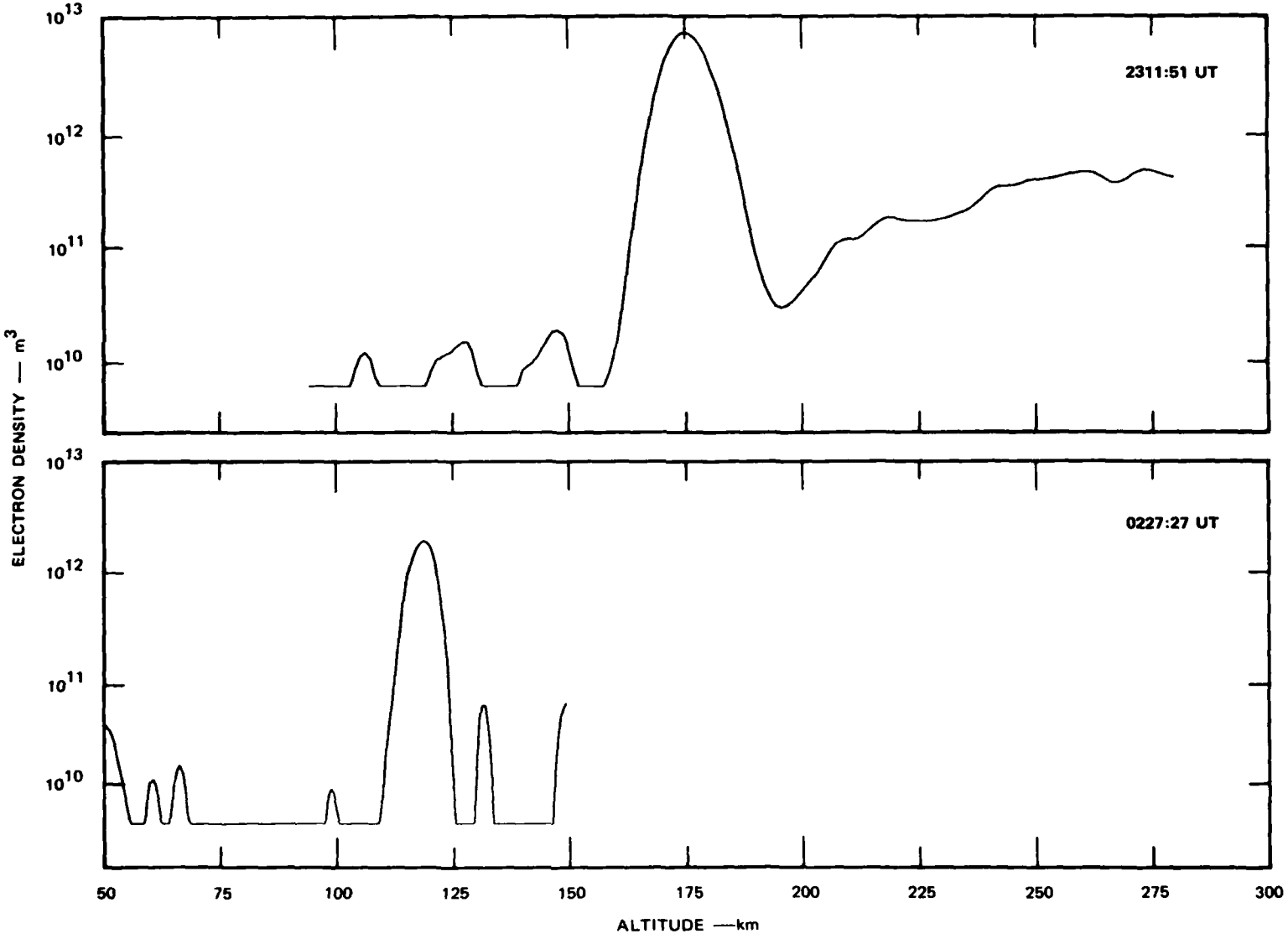

FIGURE 12 ELECTRON DENSITIES DERIVED FROM DATA IN FIGURE 11 FOR EVENT HOPE

shows the same data after the system noise, normalized to 2, has been subtracted, the range correction has been made, and the conversion to electron density has been completed. The ionosphere background above 200 km is evident. The vertical profile of the ion cloud at 0227:27 UT seems narrower than that at 2311:51 UT. This may not be the case, however, because the radar beam traversed the ion cloud at a very low-elevation angle and the apparent narrow vertical extent of the ion cloud may be caused by the radar beam entering through one side of the cloud and leaving through the other side of the ion cloud. In other words, the cloud may extend above and below 120 km and remain outside the radar beam. This problem should be studied in greater detail, in case another barium release program is contemplated.

Vertical profiles of the ion cloud were formed by choosing the maximum electron density at a given height from a set of approximately 40 to 50 antenna-beam positions. We can reasonably assume that these profiles show the electron density along the magnetic field line with the maximum electron content. Some words of caution should be added because the discrete number of antenna beam positions used during tracking do not assure that all the points along the magnetic field line of interest have been observed and measured. The resulting vertical profiles are shown in Figures 13, 14, 15, and 16 for various times.

The first vertical profile at 2325 UT is about 18 min after release and the 3-dB width is 20 km. As the ion cloud grows older and drops to lower altitudes, the three-dB width narrows to 12 km at 2404 UT, to 10 km at 2417 UT, and to about 7 km after 0220 UT. This decrease of the ionization in the vertical direction should be investigated further to verify whether it is caused by the geometric configurations of the observations since the horizontal range combined with the low altitude require every low-elevation pointing of the radar beam. A somewhat different view of this vertical extent of the ion cloud is seen in the next section, devoted to Event IRIS.

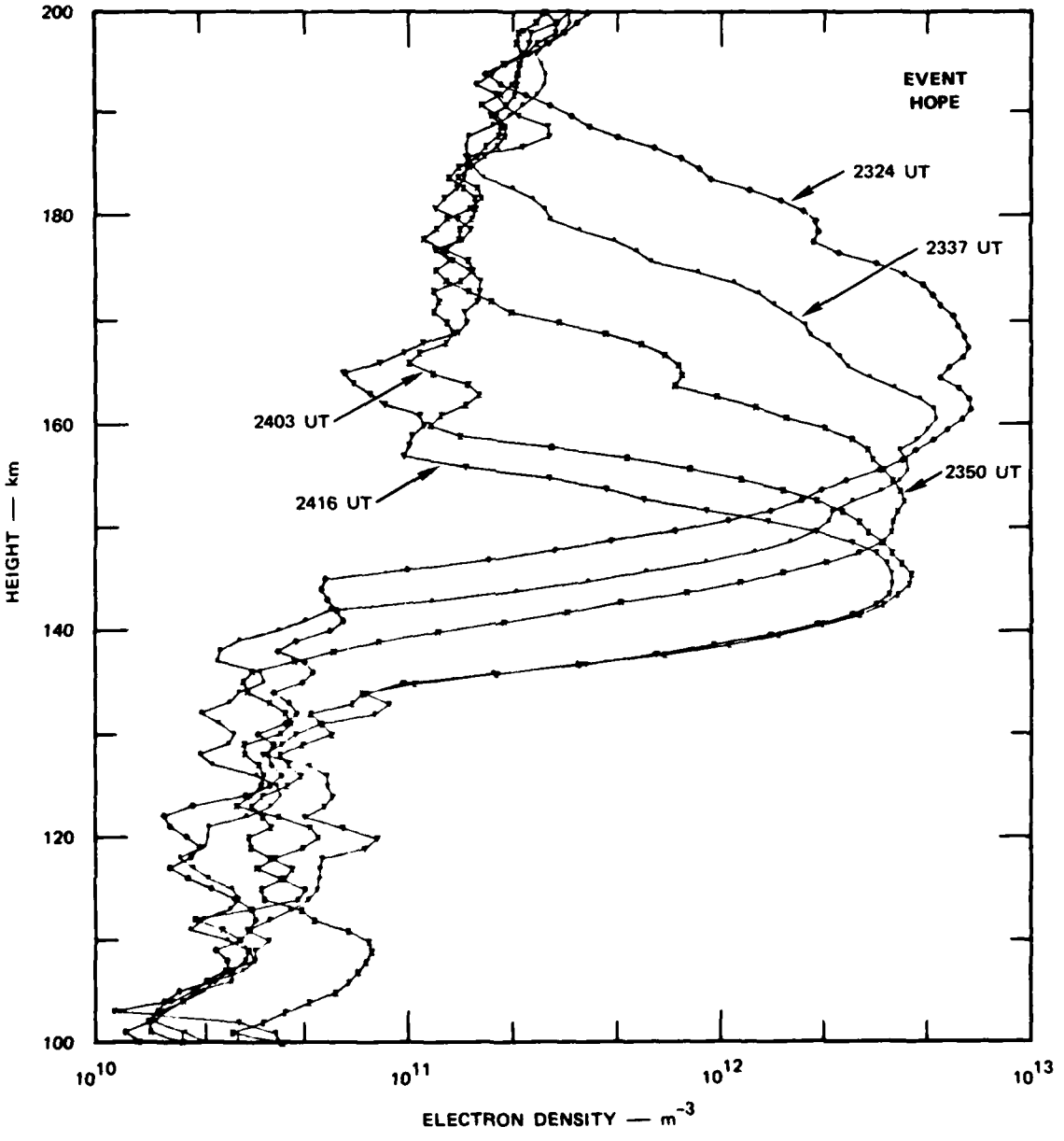

FIGURE 13 VERTICAL ELECTRON DENSITY PROFILES OF EVENT HOPE AT VARIOUS TIMES

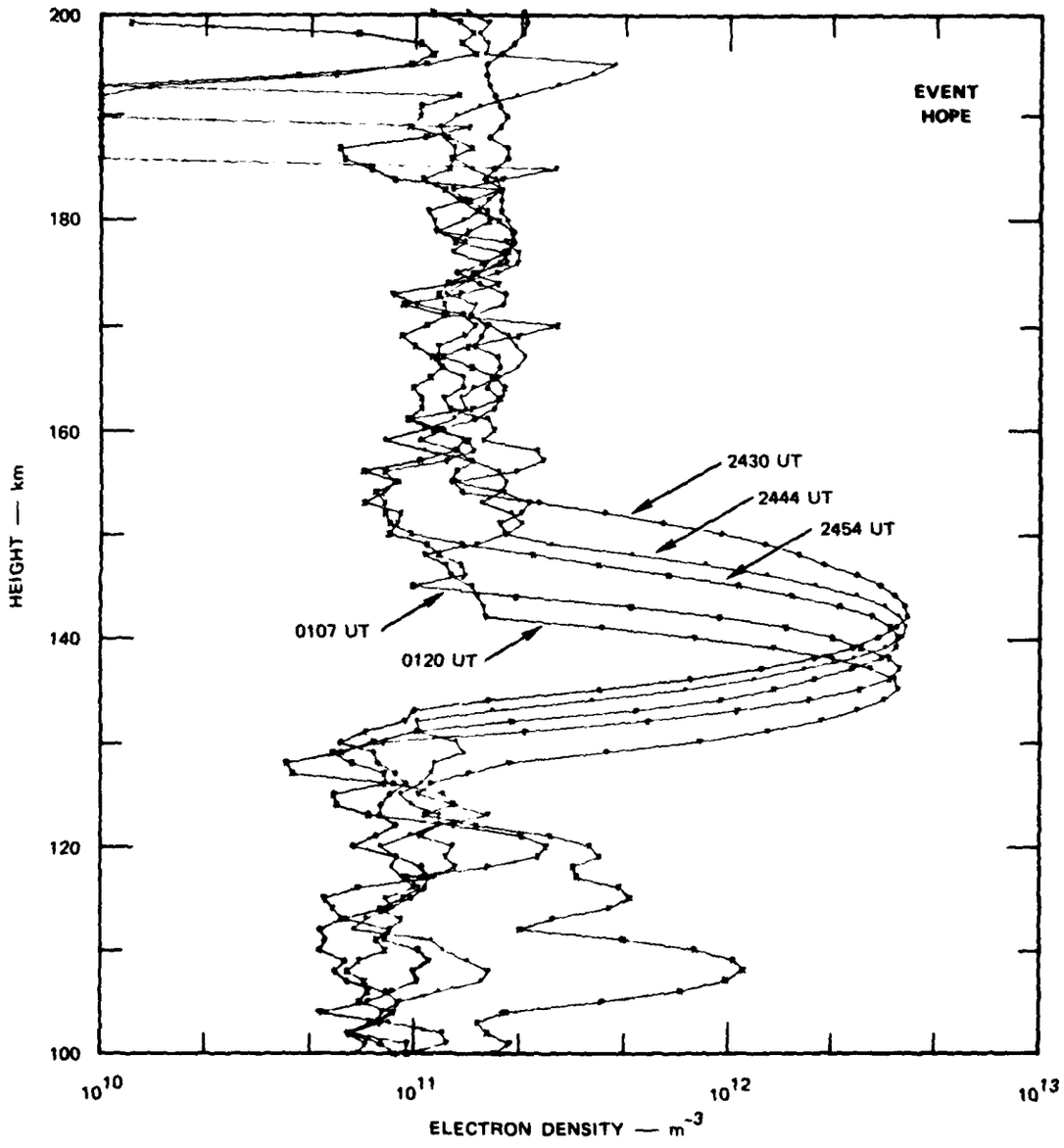

FIGURE 14 VERTICAL ELECTRON DENSITY PROFILES OF EVENT HOPE AT VARIOUS TIMES

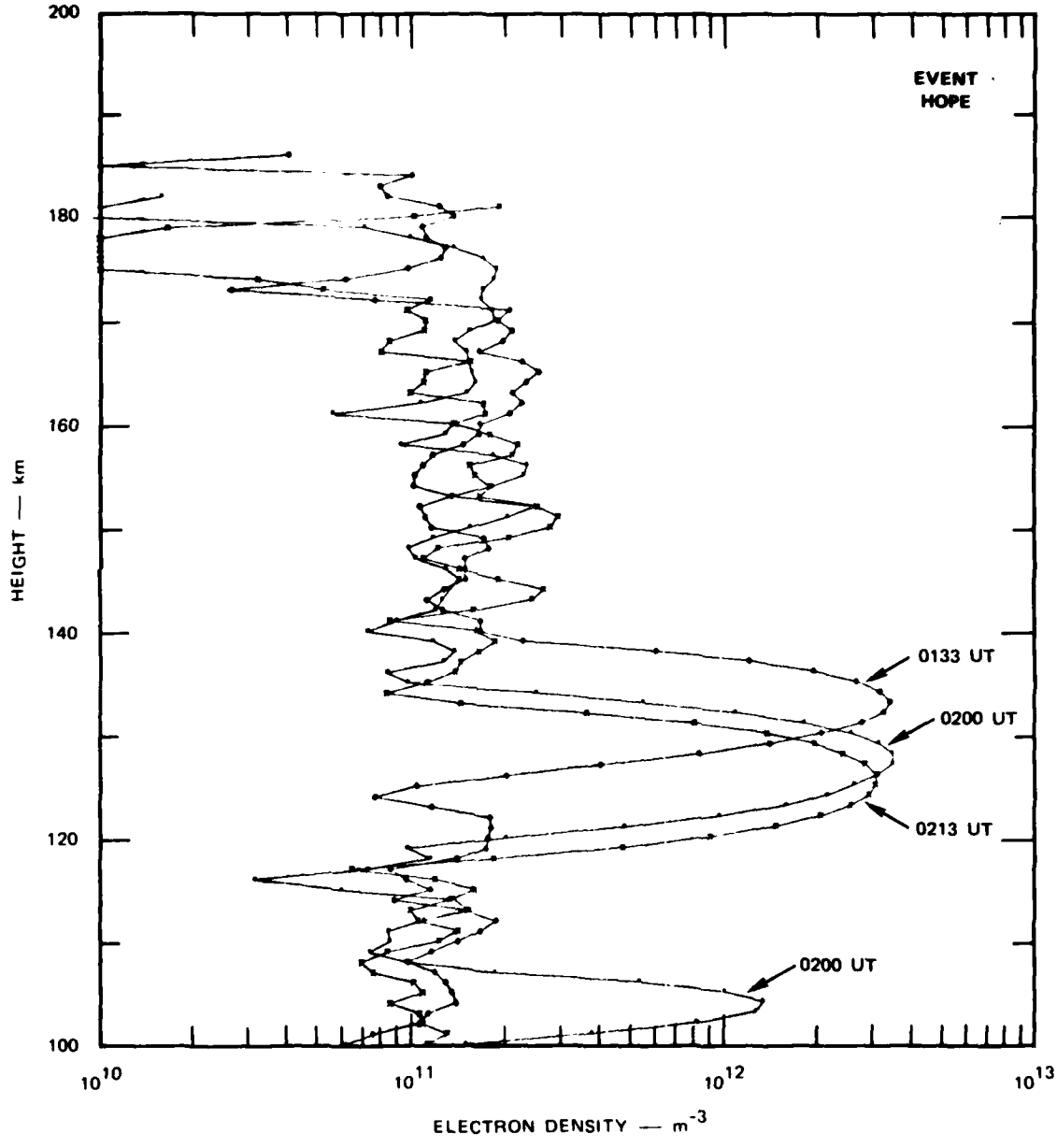

FIGURE 15 VERTICAL ELECTRON DENSITY PROFILES OF EVENT HOPE AT VARIOUS TIMES

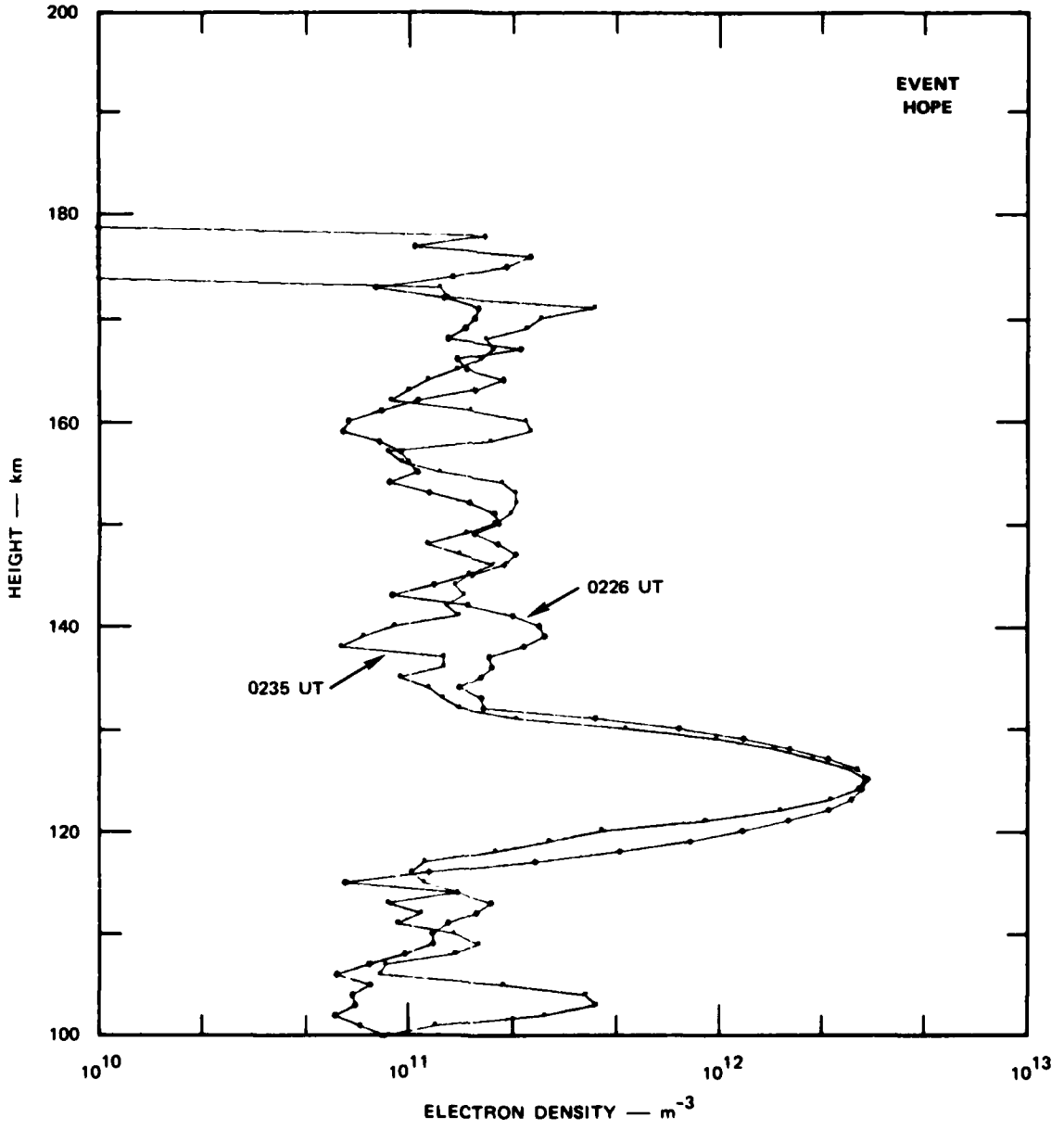

FIGURE 16 VERTICAL ELECTRON DENSITY PROFILES OF EVENT HOPE AT LATE TIMES

V EVENT IRIS

The ground track of Event IRIS is shown in Figure 17. The ion cloud location was well established about 10 or 15 min after release. The motion of the ion cloud was very steady throughout the period observation, and the average velocity was 26 m/s southward and 18 m/s eastward. This drift velocity carried the ion cloud out of the preset sampling range of the radar about 90 min after release.

The maximum electron density as a function of time is shown in Figure 18. The low electron densities during the first few minutes after release show that the radar was not pointing to the center of the ion cloud. When the ion cloud was found and the radar zeroed in on the densest part of the ion cloud, the electron density climbed up to 8×10^{12} el/m^3. The drop in electron density after T + 80 min and after T + 100 min was caused by pointing problems when the cloud drifted out of range and when the operator tried to change the preset range limits for the electron density measurements. The drop in electron density between T + 20 min and T + 30 min, however, seems to be an actual change in the ion cloud itself, since the track was well established at this time.

The altitude of the ion cloud is shown in Figure 19. The anomalies in these data define the times at which problems were encountered during the tracking of the ion cloud. The data before T + 10 min and after T + 75 min are very erratic with very wide scatter in the points. The narrow spread of data between T + 10 min and T + 75 min indicates that during this period good quality data were obtained.

Vertical profiles of the ion cloud at various times are shown in Figure 20 and the narrowing of the ion cloud in the vertical direction as the ion cloud reaches lower altitudes is not as obvious for Event IRIS as it was for Event HOPE. However, the measurements of Event IRIS do not span as large a period or as large a difference in height. The vertical

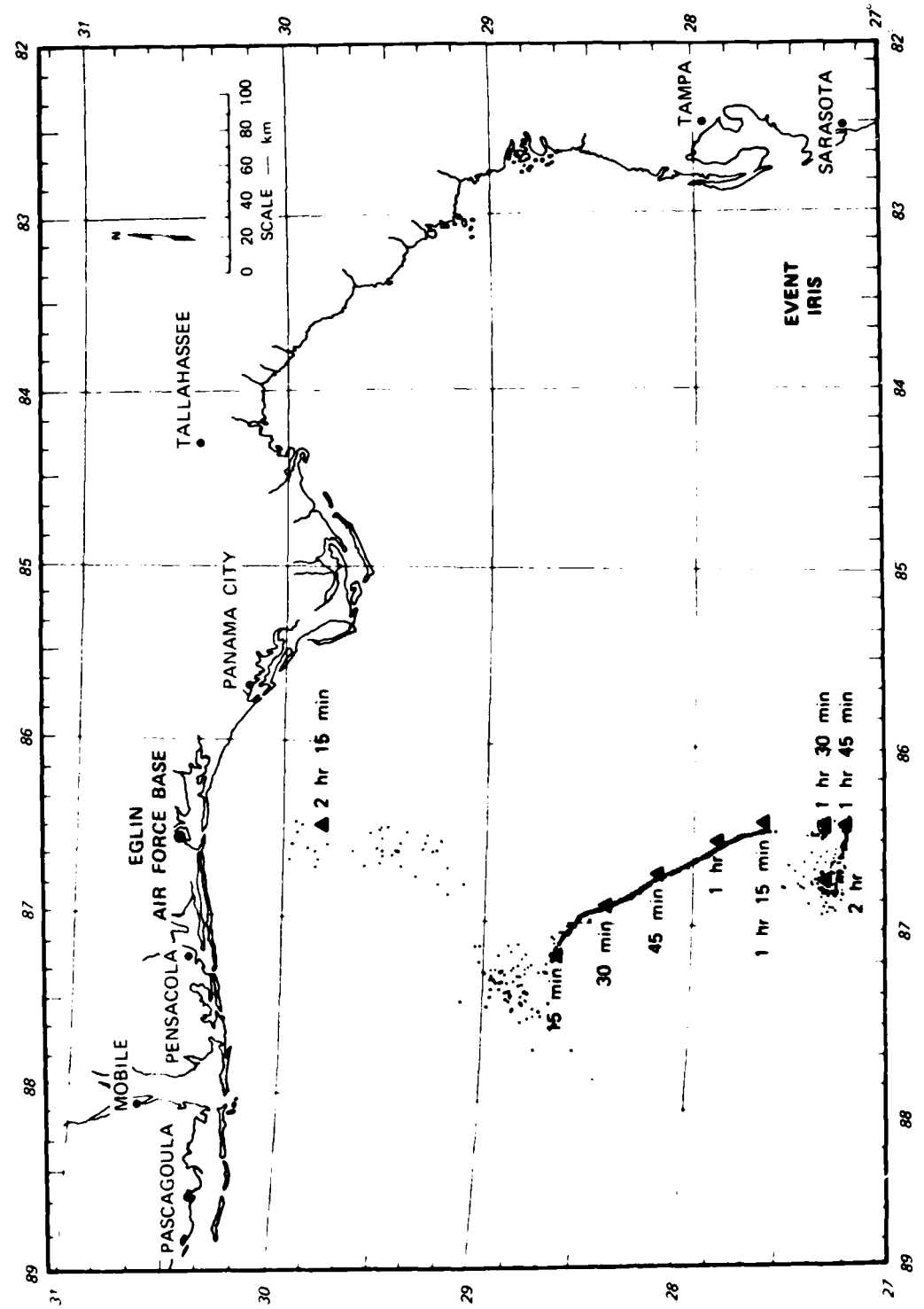

FIGURE 17 HORIZONTAL TRACK OF EVENT IRIS

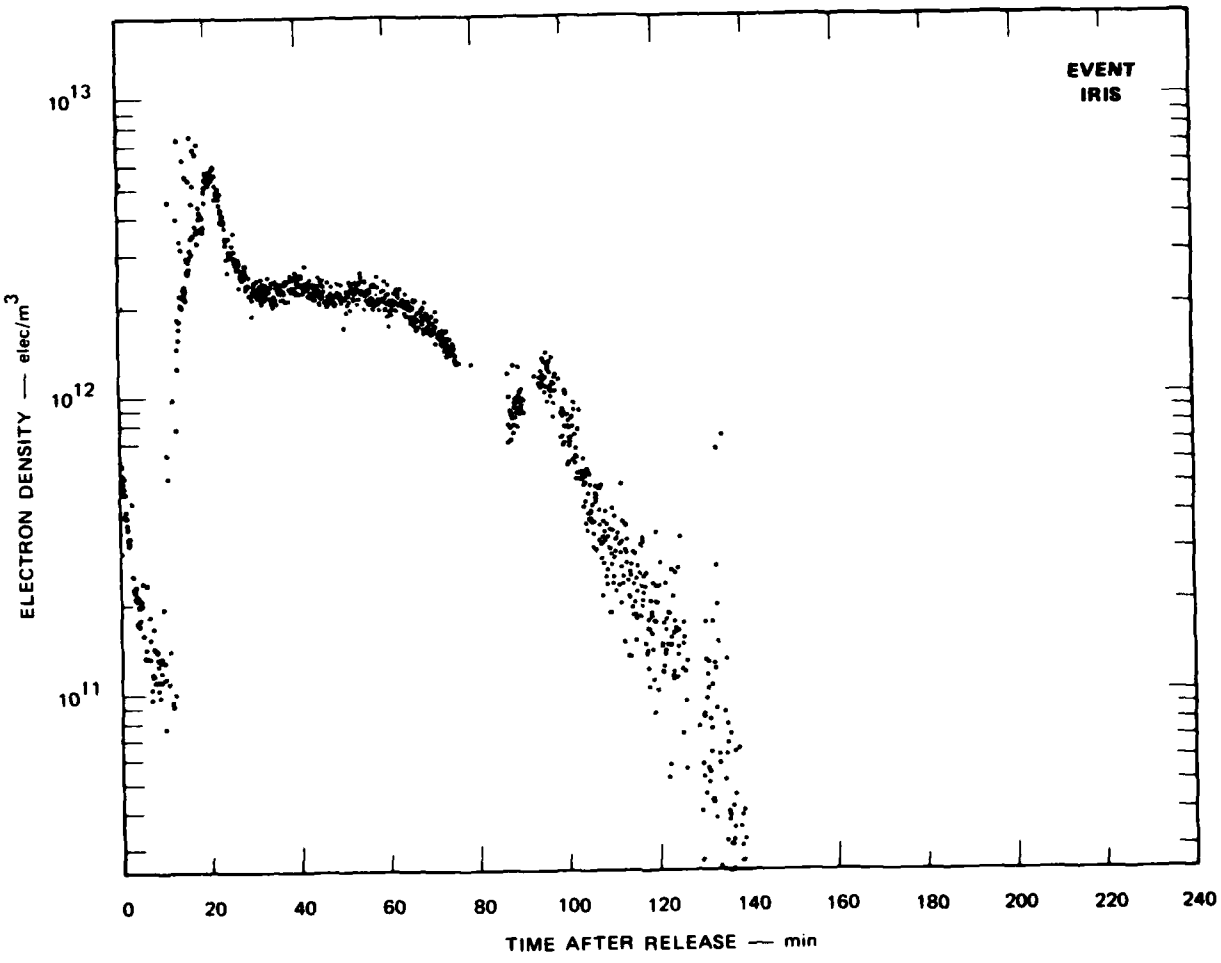

FIGURE 18 MAXIMUM MEASURED ELECTRON DENSITY OF EVENT IRIS AS A FUNCTION OF TIME

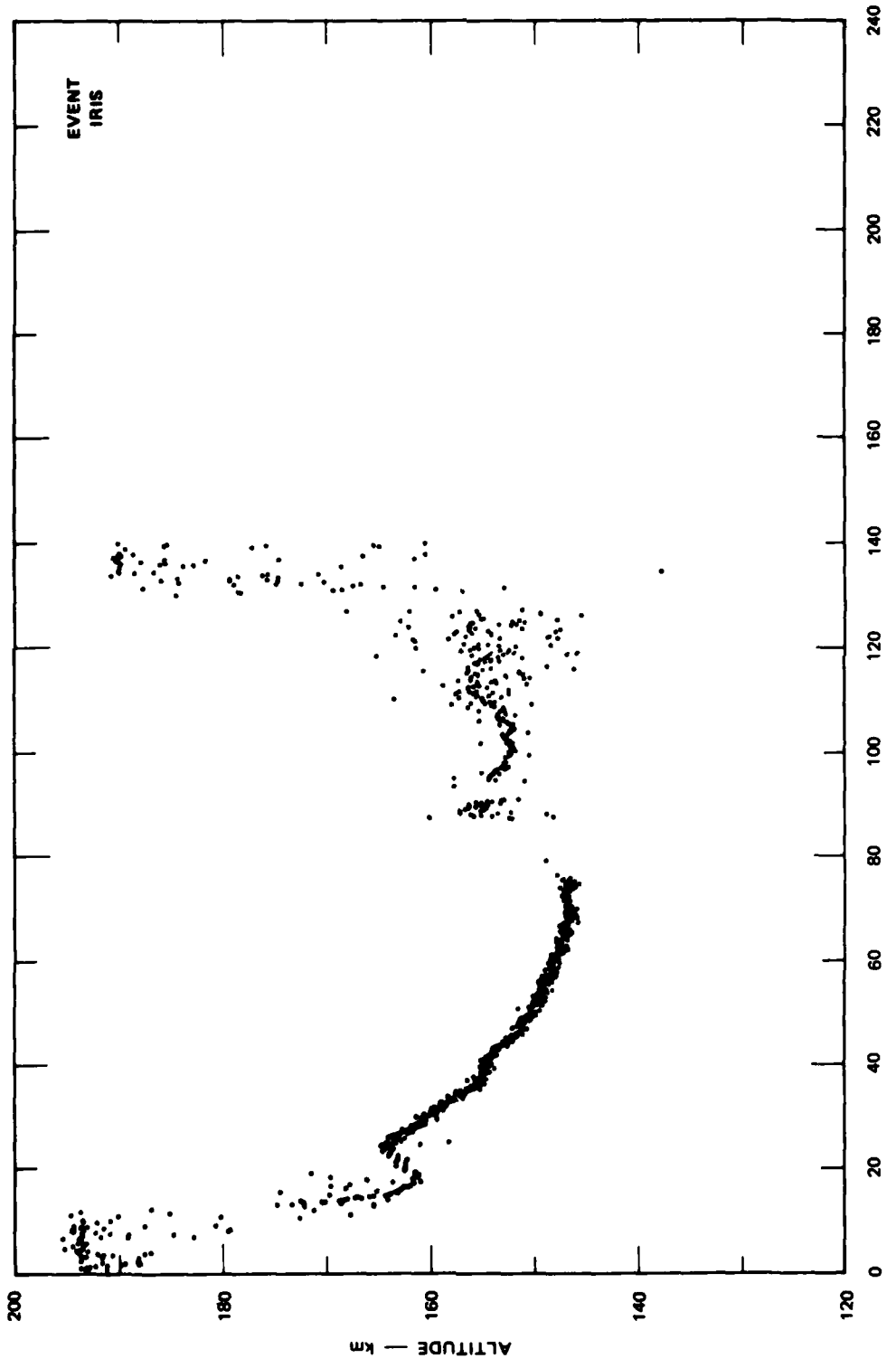

FIGURE 19 ALTITUDE DATA OF EVENT IRIS AS A FUNCTION OF TIME

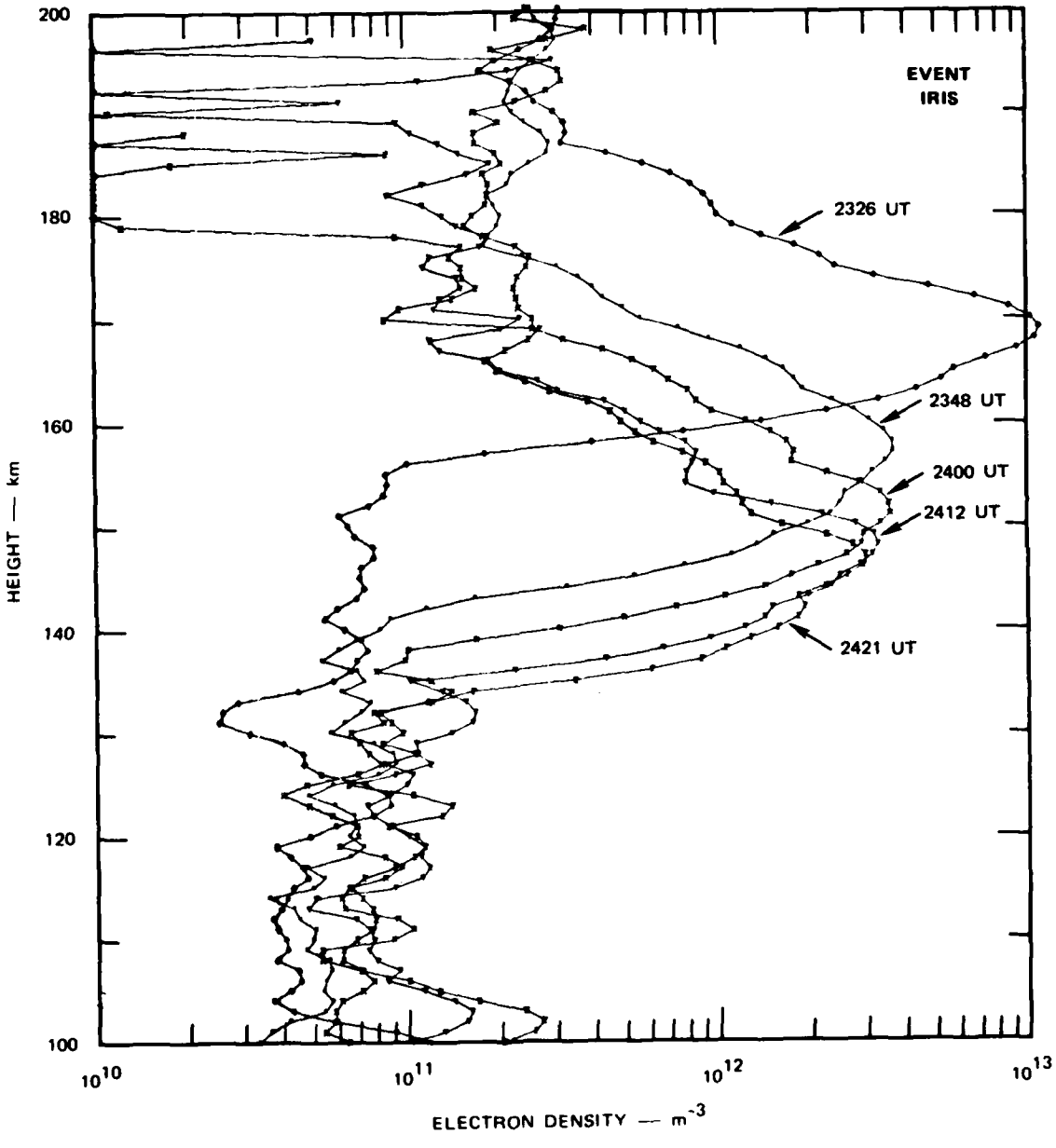

FIGURE 20 VERTICAL ELECTRON DENSITY PROFILES OF EVENT IRIS AT VARIOUS TIMES

narrowing of the ion cloud seems to be present in Figure 20, but on a smaller scale.

The horizontal shape or cut of the ion cloud has been obtained three different times, separated by about 20 min. These horizontal contours are shown in Figures 21, 22, and 23. The direction of elongation of the ion cloud is nearly perpendicular to the direction of motion of the ion cloud. The contours shown in Figure 21 show an ion cloud with a well-defined center and strong gradients. The contours of Figure 22 show a more elongated ion cloud that maintains strong gradients on its side. The third display of contours of Figure 23 shows a larger, but considerably less dense cloud with smaller gradients and a not-so-well defined shape.

We chose this later time to explore the vertical extent and shape of the ion cloud. Figure 24 shows the vertical profile of the ion cloud in the North-South vertical plane. According to Figure 22, the North-South dimension is close to the smallest dimension of the ion cloud, and certainly it is considerably smaller than the East-West dimension. Figure 24 also shows, for reference, the size of the radar beam and the area within which measurements were acquired. This area is within the limits marked as boundary for acquisition of data. The approximate direction of the Earth's magnetic field is also shown in this figure.

A few observations can be made at this point. The short vertical width of the ion cloud seems to be a real feature of this cloud: 9 km for 3-dB width. The overall shape of the ion cloud does not seem to align with the Earth's magnetic field. This last feature could be understood by saying that different regions of the ion cloud have descended to different altitudes. That is, if the northern part of the ion cloud which also happens to be the eastern part is 5 km lower than the southern part, then we can understand better the relation of the contours of Figure 24 to the magnetic field line. Again, these observations should be made with caution because of the limitations on the data acquired by the radar. The radar antenna beam uses a discrete number of positions to acquire data, and Figure 24 may be incomplete because not enough points were observed.

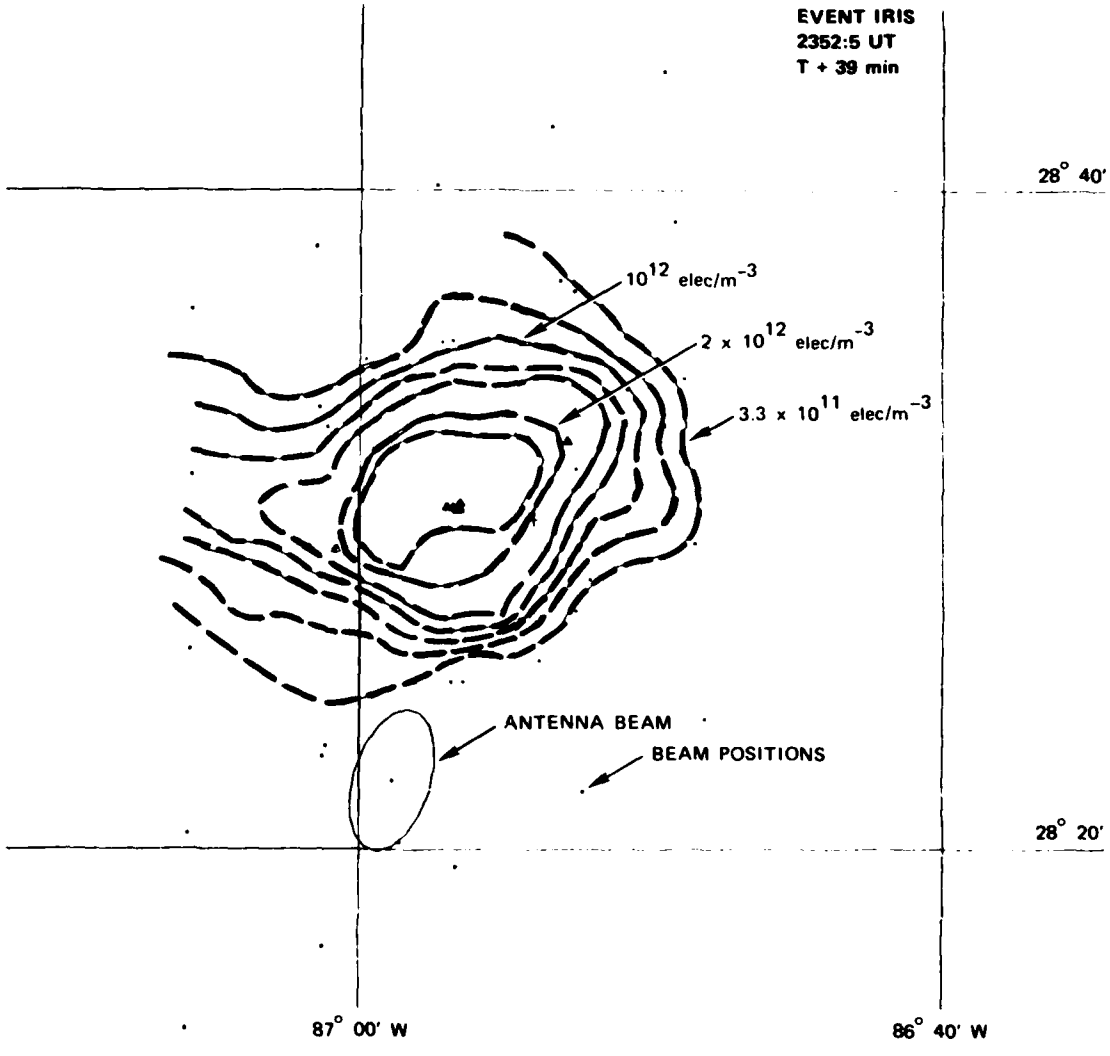

FIGURE 21 HORIZONTAL CONSTANT ELECTRON DENSITY CONTOURS AT T + 21 min

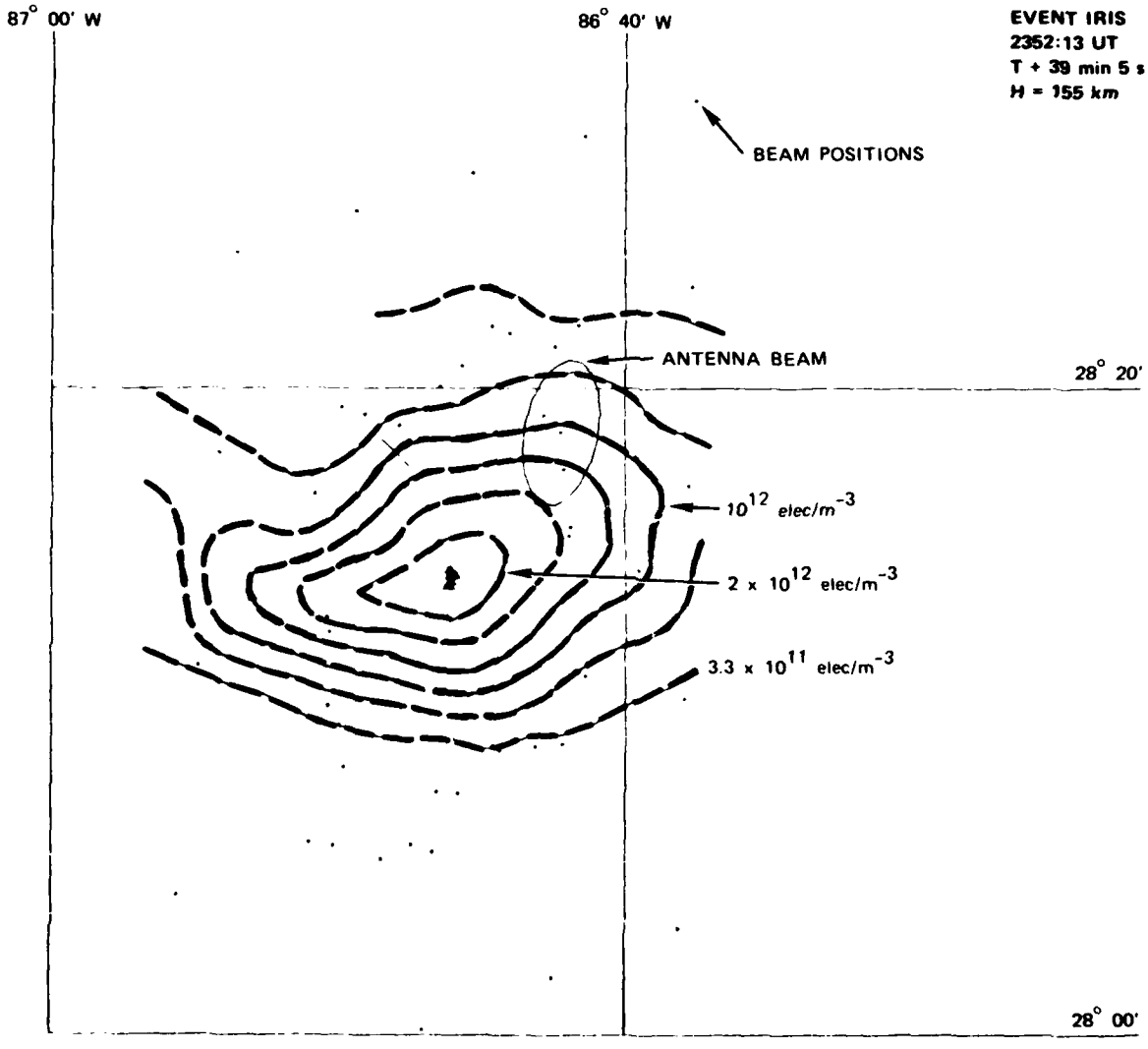

FIGURE 22 HORIZONTAL CONSTANT ELECTRON DENSITY CONTOURS OF EVENT IRIS AT T + 39 min

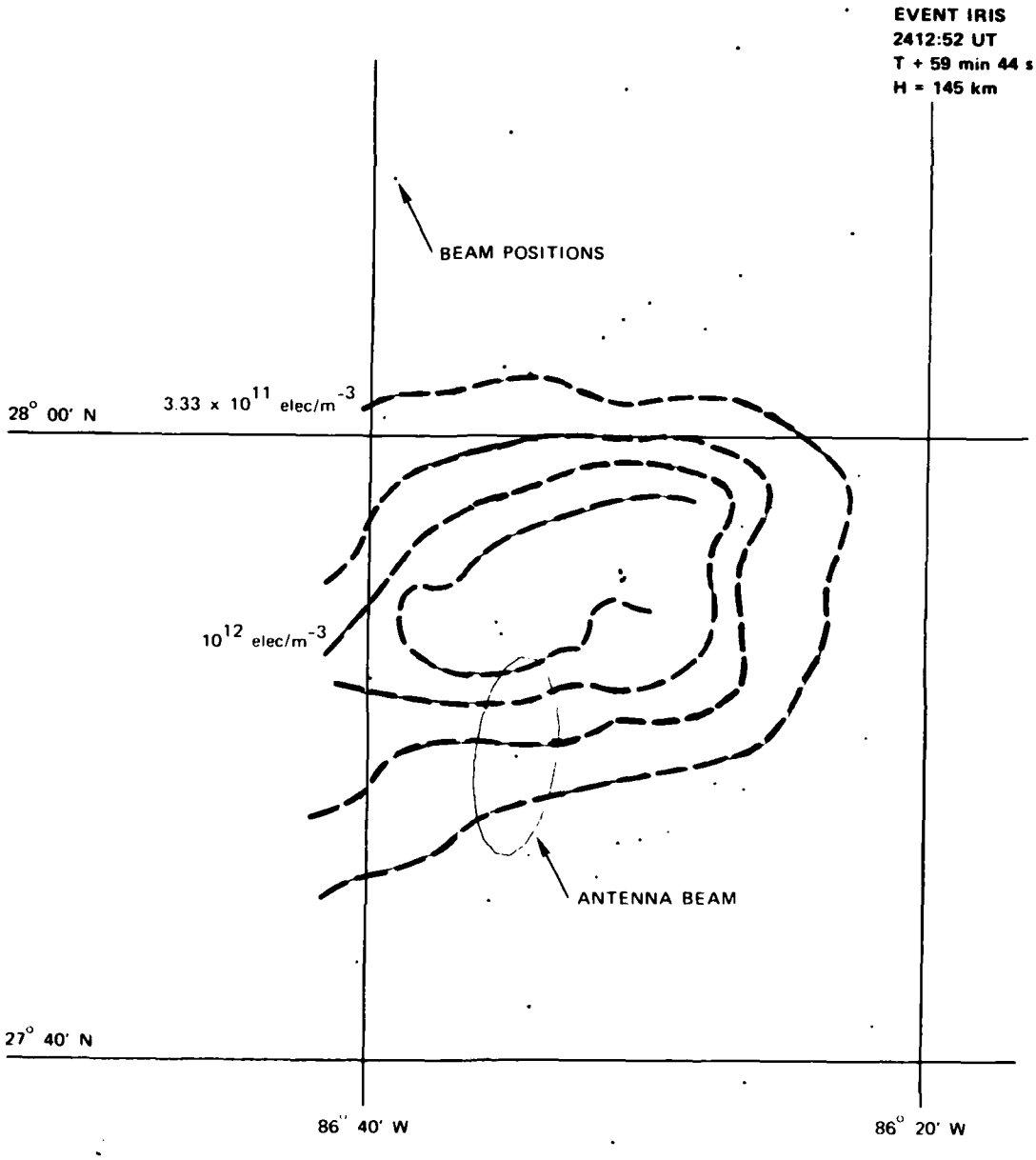

FIGURE 23 HORIZONTAL CONSTANT ELECTRON DENSITY CONTOURS OF EVENT IRIS AT T + 60 min

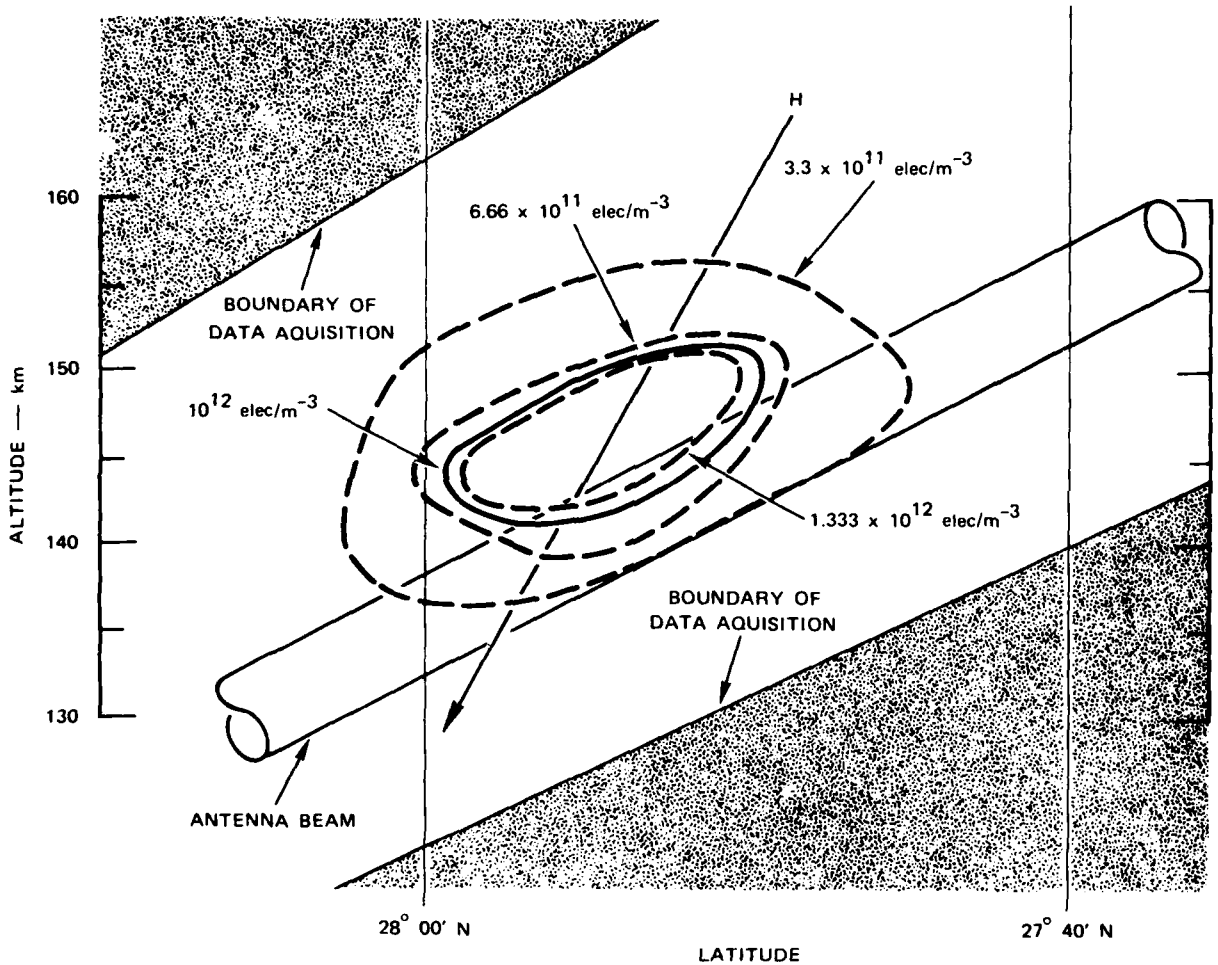

FIGURE 24 VERTICAL SLOPE OF EVENT IRIS AT 2413 UT (T + 60 min)

VI EVENT JAN

Event JAN was affected by two failures in the computer system. After a partial recovery between T + 8 min and T + 25 min, the second breakdown occurred and all efforts to reacquire the ion cloud were unsuccessful. The ground track, the altitude data, and the maximum electron density data obtained are presented in Figures 25, 26, and 27 for the sake of completeness. The very wide spread in the data points indicates the "no-track" situation that was present for most of the time.

The period of time between T + 8 min and T + 25 min may yield useful information for correlation with the probe rocket if the time for a careful data analysis is invested.

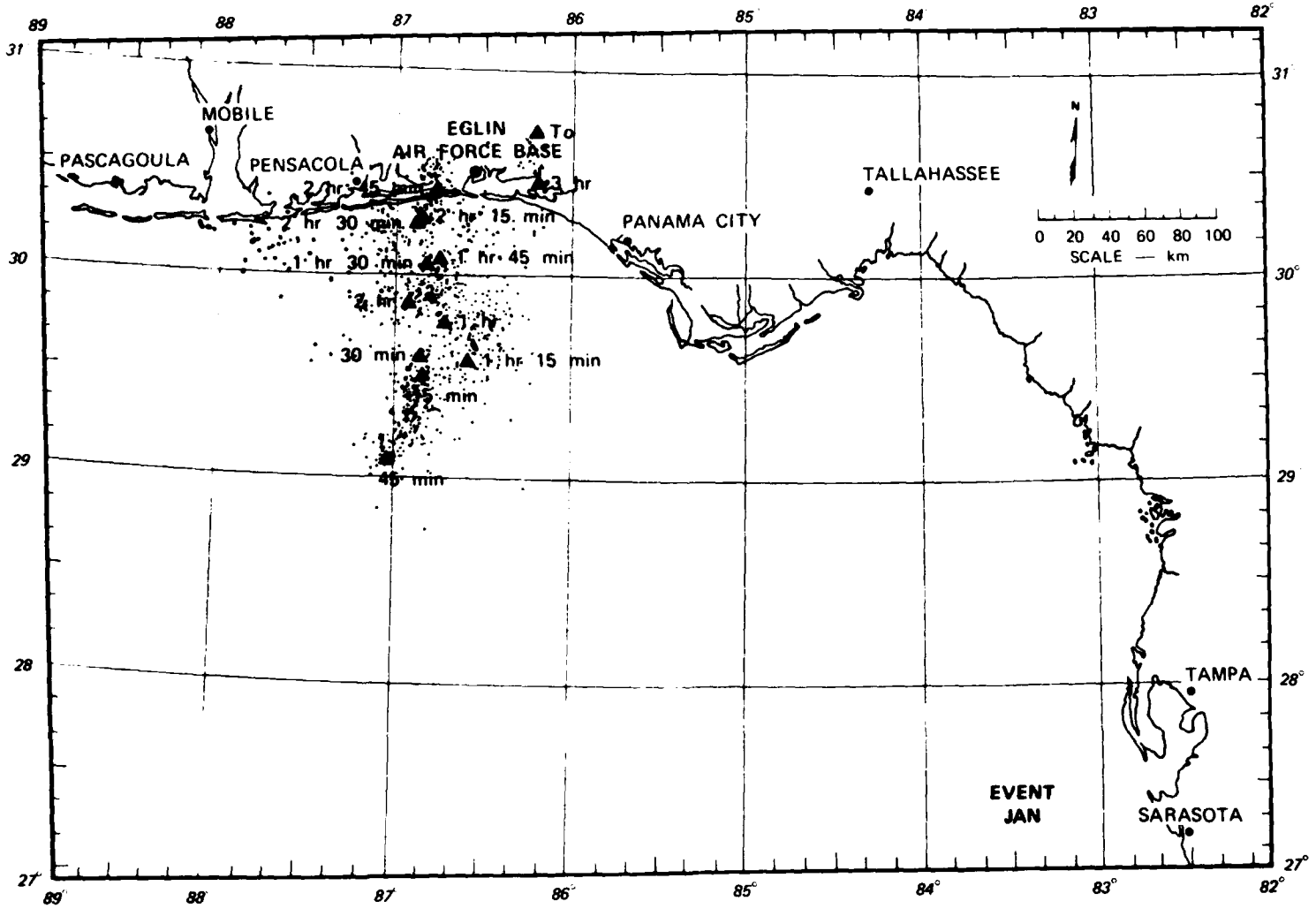

FIGURE 25 HORIZONTAL TRACK DATA OF EVENT JAN

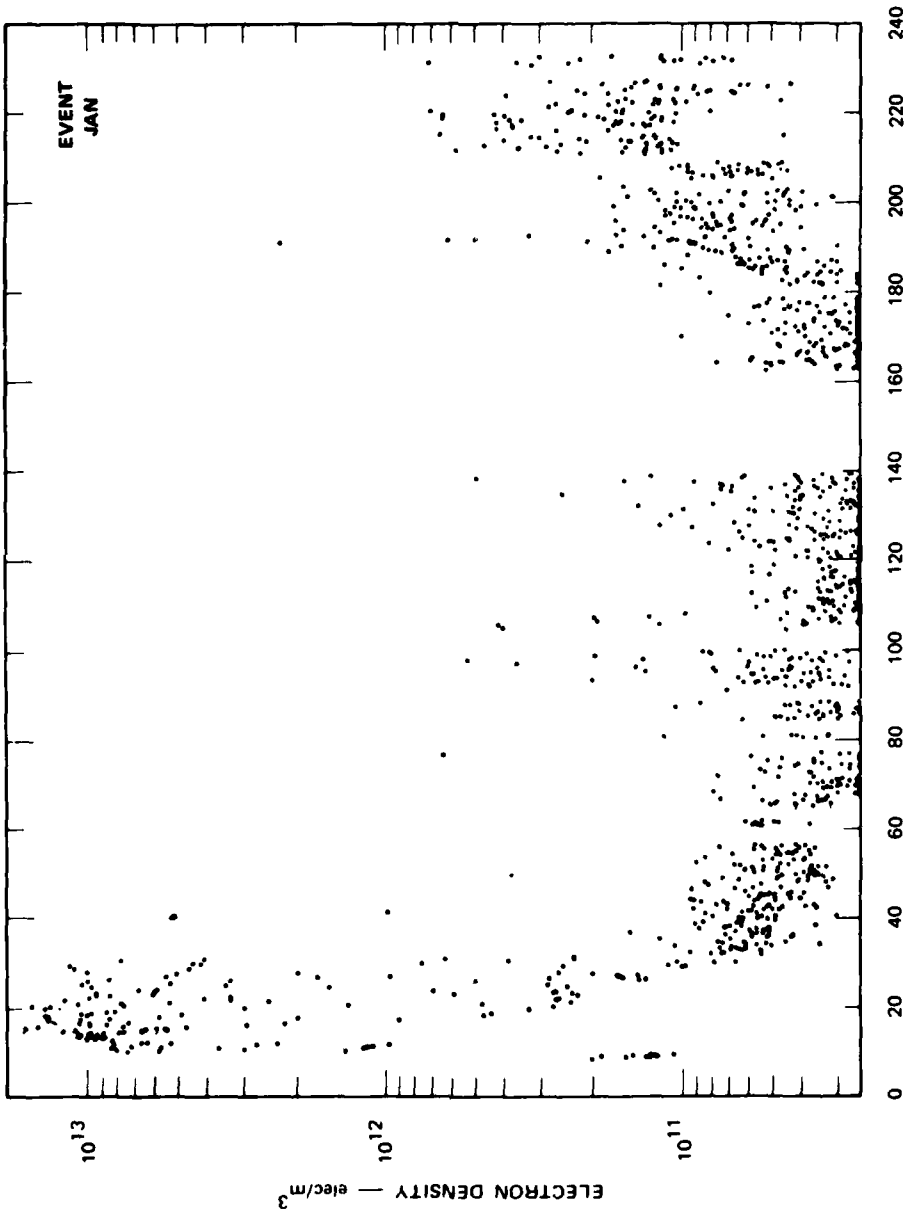

FIGURE 26 ELECTRON DENSITY DATA OF EVENT JAN AS A FUNCTION OF TIME

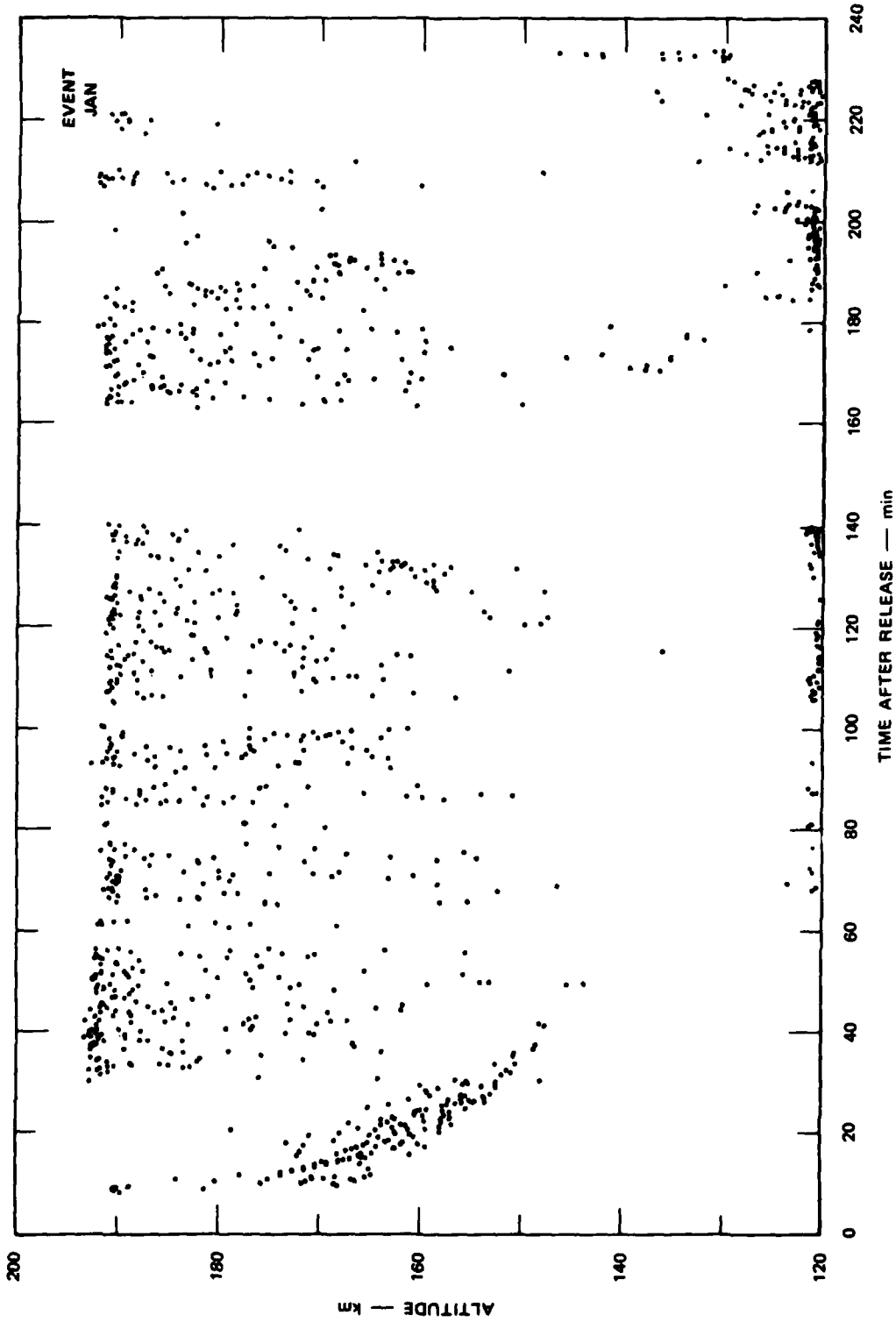

FIGURE 27 ALTITUDE DATA OF EVENT JAN AS A FUNCTION OF TIME

VII SUMMARY

During the PLACES series of experiments, Event GAIL was tracked for 2 hours, Event HOPE for 4 hours, Event IRIS for 1-1/2 hours; some data were obtained for Event JAN for about 15 min. The four-hour track of Event HOPE is the longest time a barium ion cloud has ever been tracked and the time could have been longer if we had not been constrained by the availability of the radar. Event JAN is singled out by the different extreme. It is the worst event in terms of tracking results. Thus, the PLACES series exceeded the STRESS series in one aspect and falls short of it in another.

Part of our shortcomings were caused by the aging and cumbersome computer system in the radar. The results of the programming are small compared with the effort applied. The new tracking algorithm, coupled with our new sampling hardware, did not start to work in time to be effective.

Were a new series of releases to take place in the future, several aspects of the work done could be picked up where we left off. The continuous change in the operating system of the FPS-85 will require some reprogramming. Event JAN has demonstrated the need for a more flexible tracking algorithm.

DISTRIBUTION LIST

DEPARTMENT OF DEFENSE

Assistant Secretary of Defense
Comm, Cmd, Cont & Intell
ATTN: Dir of Intelligence Sys, J. Babcock

Command & Control Technical Center
ATTN: C-650, G. Jones
ATTN: C-312, R. Mason
3 cy ATTN: C-650, W. Heidig

Defense Communications Agency
ATTN: Code 480
ATTN: Code 205
ATTN: Code 101B
ATTN: Code 480, F. Dieter

Defense Communications Engineer Center
ATTN: Code R410, N. Jones
ATTN: Code R123

Defense Intelligence Agency
ATTN: Dir
ATTN: DB-4C, E. O'Farrell
ATTN: DB, A. Wise
ATTN: DT-1B
ATTN: DC-7B

Defense Nuclear Agency
ATTN: NAFD
ATTN: STNA
ATTN: RAEE
ATTN: NATD
3 cy ATTN: RAAE
4 cy ATTN: TITL

Defense Technical Information Center
12 cy ATTN: DD

Field Command
Defense Nuclear Agency
ATTN: FCPR, J. T. McDaniel

Field Command
Defense Nuclear Agency
Livermore Branch
ATTN: FCPRL

Interservice Nuclear Weapons School
ATTN: TTV

Joint Chiefs of Staff
ATTN: C3S
ATTN: C3S, Evaluation Office

Joint Strat Tgt Planning Staff
ATTN: JLA
ATTN: JLTW-2

National Security Agency
ATTN: W-32, O. Bartlett
ATTN: B-3, F. Leonard
ATTN: R-52, J. Skillman

Under Secretary of Defense for Rsch & Engrg
ATTN: Strategic & Space Sys (OS)

DEPARTMENT OF DEFENSE (Continued)

WWMCCS System Engineering Org
ATTN: J. Hoff

DEPARTMENT OF THE ARMY

Assistant Chief of Staff for Automation & Comm
Department of the Army
ATTN: DAAC-ZT, P. Kenny

Atmospheric Sciences Laboratory
U.S. Army Electronics R&D Command
ATTN: DELAS-EO, F. Niles

BMD Advanced Technology Center
Department of the Army
ATTN: ATC-T, M. Capps
ATTN: ATC-O, W. Davies

BMD Systems Command
Department of the Army
2 cy ATTN: BMDSC-HW

Deputy Chief of Staff for Ops & Plans
Department of the Army
ATTN: DAMO-RQC

Harry Diamond Laboratories
Department of the Army
ATTN: DELHD-N-RB, R. Williams
ATTN: Chief, Div 20000
ATTN: DELHD-I-TL, M. Weiner

U.S. Army Chemical School
ATTN: ATZN-CM-CS

U.S. Army Comm-Elec Engrg Instal Agency
ATTN: CCC-EMEO-PED, G. Lane
ATTN: CCC-CED-CCO, W. Neuendorf

U.S. Army Communications Command
ATTN: CC-OPS-W
ATTN: CC-OPS-WR, H. Wilson

U.S. Army Communications R&D Command
ATTN: DRDCO-COM-RY, W. Kesselman

U.S. Army Foreign Science & Tech Ctr
ATTN: DRXST-SD

U.S. Army Materiel Dev & Readiness Cmd
ATTN: DRCLDC, J. Bender

U.S. Army Missile Intelligence Agency
ATTN: YSE, J. Gamble

U.S. Army Nuclear & Chemical Agency
ATTN: Library

U.S. Army Satellite Comm Agency
ATTN: Document Control

U.S. Army TRADOC Sys Analysis Actvy
ATTN: ATAA-TDC
ATTN: ATAA-PL
ATTN: ATAA-TCC, F. Payan, Jr

DEPARTMENT OF THE NAVY

COMSPTEVFOR
Department of the Navy
ATTN: Code 605, R. Berg

Joint Cruise Missiles Project Ofc
Department of the Navy
ATTN: JCMG-707

Naval Air Development Center
ATTN: Code 6091, M. Setz

Naval Air Systems Command
ATTN: PMA 271

Naval Electronic Systems Command
ATTN: PME 106-4, S. Kearney
ATTN: PME 117-2013, G. Burnhart
ATTN: PME 117-211, B. Kruger
ATTN: Code 3101, T. Hughes
ATTN: PME 106-13, T. Griffin
ATTN: PME 117-20
ATTN: Code 501A

Naval Intelligence Support Ctr
ATTN: NISC-50

Naval Ocean Systems Center
ATTN: Code 532, R. Pappert
ATTN: Code 532, J. Bickel
ATTN: Code 5322, M. Paulson
3 cy ATTN: Code 5323, J. Ferguson

Naval Research Laboratory
ATTN: Code 7550, J. Davis
ATTN: Code 4187
ATTN: Code 7500, B. Wald
ATTN: Code 4700, T. Coffey
ATTN: Code 7950, J. Goodman
ATTN: Code 4780, S. Ossakow

Naval Space Surveillance System
ATTN: J. Burton

Naval Surface Weapons Center
ATTN: Code F31

Naval Telecommunications Command
ATTN: Code 341

Office of Naval Research
ATTN: Code 465
ATTN: Code 421
ATTN: Code 420

Office of the Chief of Naval Operations
ATTN: OP 65
ATTN: OP 941D
ATTN: OP 981N

Strategic Systems Project Office
Department of the Navy
ATTN: NSP-43
ATTN: NSP-2722, F. Wimberly
ATTN: NSP-2141

DEPARTMENT OF THE AIR FORCE

Aerospace Defense Command
Department of the Air Force
ATTN: DC, T. Long

Air Force Geophysics Laboratory
ATTN: OPR, H. Gardiner
ATTN: OPR-1
ATTN: LKB, K. Champion
ATTN: OPR, A. Stair
ATTN: S. Basu
ATTN: PHP
ATTN: PHI, J. Buchau
ATTN: R. Thompson

Air Force Weapons Laboratory
Air Force Systems Command
ATTN: SUL
ATTN: NTYC
ATTN: NTN

Air Force Wright Aeronautical Lab
ATTN: W. Hunt
ATTN: A. Johnson

Air Logistics Command
Department of the Air Force
ATTN: OO-ALC/MM

Air University Library
Department of the Air Force
ATTN: AUL-LSE

Air Weather Service, MAC
Department of the Air Force
ATTN: DNXP, R. Babcock

Assistant Chief of Staff
Studies & Analyses
Department of the Air Force
ATTN: AF/SASC, C. Rightmeyer
ATTN: AF/SASC, W. Keaus

Ballistic Missile Office
Air Force Systems Command
ATTN: ENSN, J. Allen

Deputy Chief of Staff
Operations Plans and Readiness
Department of the Air Force
ATTN: AFXOKS
ATTN: AFXOXFD
ATTN: AFXOKT
ATTN: AFXOKCD

Deputy Chief of Staff
Research, Development, & Acq
Department of the Air Force
ATTN: AFRDS
ATTN: AFRDSS
ATTN: AFRDSP

Electronic Systems Division
Department of the Air Force
ATTN: DCKC, J. Clark

DEPARTMENT OF THE AIR FORCE (Continued)

Electronic Systems Division
Department of the Air Force
ATTN: OCT-4, J. Deas

Electronic Systems Division
Department of the Air Force
ATTN: YSEA
ATTN: YSM, J. Kobelski

Foreign Technology Division
Air Force Systems Command
ATTN: TQTD, B. Ballard
ATTN: NIIS, Library

Space Division
Department of the Air Force
ATTN: SKA, D. Bolin
ATTN: SKY, C. Kennedy

Space Division
Department of the Air Force
ATTN: YGJB, W. Mercer

Space Division
Department of the Air Force
ATTN: E. Butt

Rome Air Development Center
Air Force Systems Command
ATTN: OCS, V. Coyne
ATTN: TSLD

Rome Air Development Center
Air Force Systems Command
ATTN: EEP

Strategic Air Command
Department of the Air Force
ATTN: DCXT
ATTN: DCXR, T. Jorgensen
ATTN: NRT
ATTN: XPFS
ATTN: DCX

OTHER GOVERNMENT AGENCIES

Central Intelligence Agency
ATTN: OSWR/NED

Department of Commerce
National Bureau of Standards
ATTN: Sec Ofc for R. Moore

Department of Commerce
National Oceanic & Atmospheric Admin
ATTN: R. Grubb

Institute for Telecommunications Sciences
National Telecommunications & Info Admin
ATTN: W. Utlaut
ATTN: A. Jean
ATTN: L. Berry

DEPARTMENT OF ENERGY CONTRACTORS

EG&G, Inc
Los Alamos Division
ATTN: D. Wright
ATTN: J. Colvin

DEPARTMENT OF ENERGY CONTRACTORS (Continued)

Lawrence Livermore National Lab
ATTN: L-389, R. Ott
ATTN: L-31, R. Hager
ATTN: Technical Info Dept, Library

Los Alamos National Laboratory
ATTN: MS 664, J. Zinn
ATTN: D. Simons
ATTN: P. Keaton
ATTN: C. Westervelt
ATTN: E. Jones
ATTN: R. Taschek
ATTN: MS 670, J. Hopkins

Sandia National Laboratories
Livermore Laboratory
ATTN: T. Cook
ATTN: B. Murphey

Sandia National Lab
ATTN: Org 4241, T. Wright
ATTN: D. Thornbrough
ATTN: 3141
ATTN: D. Dahlgren
ATTN: Space Project Div
ATTN: Org 1250, W. Brown

DEPARTMENT OF DEFENSE CONTRACTORS

Aerospace Corp
ATTN: I. Garfunkel
ATTN: R. Slaughter
ATTN: D. Olsen
ATTN: J. Straus
ATTN: T. Salmi
ATTN: V. Josephson
ATTN: S. Bower
ATTN: N. Stockwell

Analytical Systems Engineering Corp
ATTN: Radio Sciences

Analytical Systems Engineering Corp
ATTN: Security

Barry Research Corporation
ATTN: J. McLaughlin

BDM Corp
ATTN: L. Jacobs
ATTN: T. Neighbors

Berkeley Research Associates, Inc
ATTN: J. Workman

Betac
ATTN: J. Hirsch

Boeing Co
ATTN: M/S 42-33, J. Kennedy
ATTN: G. Hall
ATTN: S. Tashird

Booz-Allen & Hamilton, Inc
ATTN: B. Wilkinson

University of California at San Diego
ATTN: H. Booker

DEPARTMENT OF DEFENSE CONTRACTORS (Continued)

Charles Stark Draper Lab, Inc
ATTN: J. Gilmore
ATTN: D. Cox

Communications Satellite Corp
ATTN: D. Fang

Computer Sciences Corp
ATTN: F. Eisenbarth

Comsat Labs
ATTN: G. Hyde

Cornell University
ATTN: M. Kelly
ATTN: D. Farley, Jr

E-Systems, Inc
ATTN: R. Berezdivin

Electrospace Systems, Inc
ATTN: H. Logston

Esl, Inc
ATTN: J. Marshall

General Electric Co
ATTN: A. Harcar

General Electric Co
ATTN: A. Steinmayer
ATTN: C. Zierdt

General Electric Co
ATTN: F. Reibert

General Electric Co
ATTN: G. Millman

General Research Corp
ATTN: J. Ise, Jr
ATTN: J. Garbarino

Harris Corp
ATTN: E. Knick

Horizons Technology, Inc
ATTN: R. Kruger

HSS, Inc
ATTN: D. Hansen

IBM Corp
ATTN: F. Ricci

University of Illinois
ATTN: K. Yeh

Institute for Defense Aanlyses
ATTN: H. Wolfhard
ATTN: J. Aein
ATTN: E. Bauer

International Tel & Telegraph Corp
ATTN: G. Wetmore
ATTN: Technical Library

JAYCOR
ATTN: J. Sperling

DEPARTMENT OF DEFENSE CONTRACTORS (Continued)

JAYCOR
ATTN: J. Doncarlos

Johns Hopkins University
ATTN: T. Potemra
ATTN: J. Phillips
ATTN: T. Evans
ATTN: J. Newland
ATTN: P. Komiske

Kaman Tempo
ATTN: W. Knapp
ATTN: DASIAC
ATTN: T. Stephens
ATTN: W. McNamara

Linkabit Corp
ATTN: I. Jacobs

Litton Systems, Inc
ATTN: R. Grasty

Lockheed Missiles & Space Co, Inc
ATTN: W. Imhof
ATTN: R. Johnson
ATTN: M. Walt

Lockheed Missiles & Space Co, Inc
ATTN: D. Churchill
ATTN: Dept 60-12
ATTN: C. Old

M.I.T. Lincoln Lab
ATTN: D. Towle

Martin Marietta Corp
ATTN: R. Heffner

McDonnell Douglas Corp
ATTN: W. Olson
ATTN: J. Moule
ATTN: G. Mroz
ATTN: N. Harris
ATTN: R. Halprin

Meteor Communications Consultants
ATTN: R. Leader

Mission Research Corp
ATTN: R. Hendrick
ATTN: F. Fajen
ATTN: Tech Library
ATTN: R. Bogusch
ATTN: R. Kilb
ATTN: D. Sappenfield
ATTN: S. Gutsche

Mitre Corp
ATTN: G. Harding
ATTN: A. Kymmel
ATTN: C. Callahan
ATTN: B. Adams

Mitre Corp
ATTN: M. Horrocks
ATTN: W. Foster
ATTN: J. Wheeler
ATTN: W. Hall

DEPARTMENT OF DEFENSE CONTRACTORS (Continued)

Pacific-Sierra Research Corp
ATTN: E. Field, Jr
ATTN: F. Thomas
ATTN: H. Brode

Pennsylvania State University
ATTN: Ionospheric Research Lab

Photometrics, Inc
ATTN: I. Kofsky

Physical Dynamics, Inc
ATTN: E. Fremouw

Physical Research, Inc
ATTN: R. Deliberis

R & D Associates
ATTN: R. Lelevier
ATTN: R. Turco
ATTN: B. Gabbard
ATTN: M. Gantsweg
ATTN: W. Wright
ATTN: F. Gilmore
ATTN: C. Greifinger
ATTN: H. Ory
ATTN: W. Karzas
ATTN: P. Haas

R & D Associates
ATTN: B. Yoon

Rand Corp
ATTN: C. Crain
ATTN: E. Bedrozian

Riverside Research Institute
ATTN: V. Trapani

Rockwell International Corp
ATTN: R. Buckner

Rockwell International Corp
ATTN: S. Quilici

Santa Fe Corp
ATTN: D. Paolucci

Science Applications, Inc
ATTN: SZ

DEPARTMENT OF DEFENSE CONTRACTORS (Continued)

Science Applications, Inc
ATTN: E. Straker
ATTN: C. Smith
ATTN: L. Linson
ATTN: D. Hamlin

Science Applications, Inc
ATTN: J. Cockayne

SRI International
ATTN: W. Jaye
ATTN: R. Leadabrand
ATTN: D. Neilson
ATTN: J. Petrickes
ATTN: W. Chesnut
ATTN: R. Livingston
ATTN: R. Tsunoda
ATTN: G. Price
ATTN: C. Rino
ATTN: A. Burns
ATTN: G. Smith
ATTN: M. Baron
4 cy ATTN: V. Gonzalez

Sylvania Systems Group
ATTN: I. Kohlberg
ATTN: R. Steinhoff

Technology International Corp
ATTN: W. Boquist

Tri-Com, Inc
ATTN: D. Murray

TRW Defense & Space Sys Group
ATTN: R. Plebuch
ATTN: D. Dee

Utah State University
ATTN: K. Baker
ATTN: L. Jensen
ATTN: J. Dupnik

Visidyne, Inc
ATTN: C. Humphrey
ATTN: J. Carpenter